THEORETICAL STUDY OF BOSE-EINSTEIN CONDENSATE-BASED ATOM MICHELSON INTERFEROMETERS

by

Rudra Prasad Kafle, M.S.

A dissertation submitted to the faculty of

Worcester Polytechnic Institute

in partial fulfillment of the requirements for the degree of

Doctor of Philosophy

Department of Physics

Worcester Polytechnic Institute

April 2012

THEORETICAL STUDY OF BOSE-EINSTEIN CONDENSATE-BASED ATOM MICHELSON INTERFEROMETERS

DECLARATION

I, Rudra Prasad Kafle, declare that this dissertation titled *Theoretical Study Of Bose-Einstein Condensate-Based Atom Michelson Interferometers* and the work presented in it are my own.

04/24/2012 

Date Rudra Prasad Kafle, M.S.

GRADUATE COMMITTEE APPROVAL

This dissertation submitted by Rudra Prasad Kafle has been read by each member of the following graduate committee and by majority vote has been found to be satisfactory.

04/24/2012 

Date Alex A. Zozulya, PhD Advisor
Professor, Department of Physics, Worcester Polytechnic Institute

24 April 2012 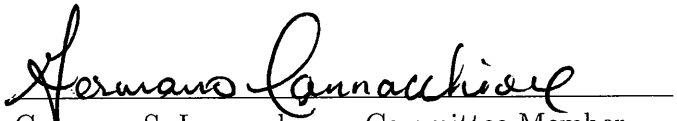

Date Germano S. Iannacchione, Committee Member
Associate Professor and Head, Department of Physics, Worcester Polytechnic Institute

04/24/2012 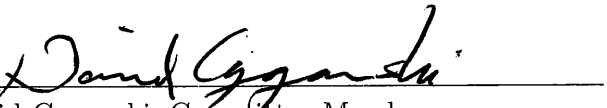

Date David Cyganski, Committee Member
Professor, Department of Electrical, Computer, and Robotics Engineering, Worcester Polytechnic Institute

ABSTRACT

Atom interferometers and gyroscopes are highly sensitive atom-optical devices which are capable to measure inertial, gravitational, electric, and magnetic fields and to sense rotations. Theoretically, the signal-to-noise ratio of atomic gyroscopes is about a hundred billion times more than that of their optical counterparts for the same particle flux and the enclosed area. Ultra cold atoms from a Bose-Einstein condensate (BEC) can easily be controlled and coherently manipulated on small chips by laser pulses. Atom-optical devices will therefore play a significant role in fundamental research, precision measurements, and navigation systems.

In BEC-based atom interferometers, a BEC in a trap is split by using laser pulses, the split clouds are allowed to evolve, they are reflected, and then recombined by laser pulses to observe interference. The split clouds accumulate spatial phase because of the trap and the nonlinearity caused by atom-atom interactions. A velocity mismatch due to reflection laser pulses also introduces a phase gradient across each cloud. These factors contribute to spatial relative phase between the clouds at recombination, causing the loss of contrast of the interference fringes. The main objective of this dissertation is to study the dynamics of a split condensate in atom Michelson interferometers, investigate the effect of trap frequencies, nonlinearity, and the velocity mismatch on the contrast, and to obtain the best theoretical limit of performance in terms of the experimental parameters: trap frequencies, number of atoms, and the velocity imparted to the clouds by the splitting laser pulses.

ACKNOWLEDGMENTS

It is said that, 'No man is an island'. In the long journey of my life and in the course of my graduate studies at Worcester Polytechnic Institute (WPI), there were several people who helped mold my life. I would like to thank all of them from the bottom of my heart.

First of all, I express my deepest gratitude to my advisor Prof. Alex A. Zozulya for his excellent advising and supervision in my research and graduate studies. I appreciate Dr. James A. Stickney for his guidance in numerical techniques in the beginning years of my research.

I am indebted to the Physics Department for financial support to my graduate studies at WPI. My special thanks goes to the Department Head Prof. Germano Iannacchione for providing me with several opportunities which were atypical for a general graduate student. I have a great respect for his excellent advice and encouragement at the time that I really needed them. I would like to thank Prof. Padmanabhan K. Aravind for giving me opportunities to work with the Physics Frontiers during several summers. I appreciate the department secretaries Jacqueline Malone (Jackie), Margaret Caisse (Peggy) and Michele O'Brien for their help and support all the time. The guidance, help and encouragement of all my professors, colleagues, and friends at WPI are highly acknowledged. Actually life at WPI is more than that of a graduate student, it is more like a family!

I sincerely thank my mentor Dr. Eddy Timmermans who mentored me

and supported my research financially for the summers of 2010 and 2011 in the Center for Nonlinear Studies at Los Alamos National Laboratory. I always appreciate Prof. Yan N. Lwin from Western Illinois University for his help, support and encouragement all the time, and Dr. Ram Basnet and his family for their help during my two summer stays at Los Alamos National Laboratory.

I would like to thank the members of the graduate committee for serving in the committee and for reading my dissertation. I reached here because of help and encouragement of my teachers, colleagues, mentors, and professors of different stages of my life. I would like to express my sincere thanks to all of them.

I would like to thank my wife Laxmi and my daughter Rumani for their constant and unconditional help and support all the time. We were blessed to have our little baby Ruchir during my PhD research period. He is so playful and has added all the joys to our family. Thank you Ruchir! Last but not the least, I am so grateful for the effort, love, support, and encouragement of my father, my grandmother, my brothers and their families, my sister and her family, and my father-in-law and his family. Your love and support always energize me to move forward!

Dedicated to my parents !

Contents

List of Figures

Chapter 1

Introduction

'If quantum mechanics hasn't profoundly shocked you, you haven't understood it yet.'
- Niels Bohr

1.1 Is light a particle or a wave?

Sir Isaac Newton was one of the pioneers in almost all areas of physics. Some of his major contributions were the development of calculus, formulation of the Laws of Motion, the Laws of Gravitation, and that of Optics. He proposed the corpuscular theory of light in the last decade of the seventeenth century [1]. This theory assumes that light consists of particles like marbles in their miniature forms. He explained the rectilinear propagation of light and reflection of light from this proposition, but his theory could not explain the refraction of light satisfactorily. According to corpuscular theory, when light passes from air to water, the vertical component of the velocity would increase but the horizontal component would remain the same. Therefore, the velocity of light in water should be more than that in air. The experiments by Foucault in 1850 and Michelson in 1885 [2] showed that the speed of light in water is less than

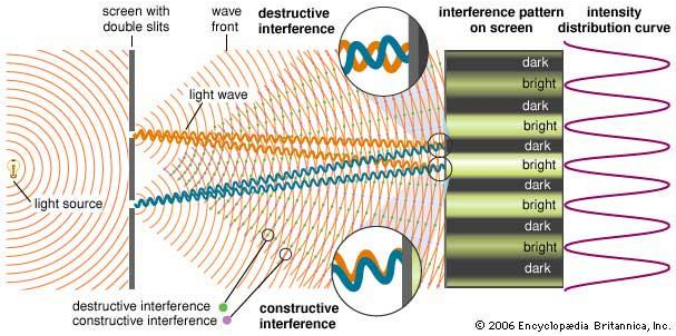

Figure 1.1 A schematic of Young's double-slit experiment (Source : Encyclopedia Britannica)

the speed of light in in air. The corpuscular theory of light also could not explain diffraction and interference phenomena. Christiaan Huygens in the late seventeenth century proposed that light should show wave-like behavior rather than particle-like behavior as proposed by Newton [2]. Huygens' wave theory of light was not accepted for about a hundred years. In 1801, Thomas Young experimentally demonstrated that light behaves like a wave through his famous double-slit experiment (see Figure 1.1). He showed that a monochromatic light passed through two very closely separated slits produced a series of bright and dark bands on the screen placed at a fairly large distance from the slits. This phenomenon that could be explained well by Huygens' wave theory of light is the interference of light waves. In Young's experiments, the slits played the role of coherent sources of the secondary wavefronts of light coming from the original monochromatic source. The waves from these two coherent sources which reached the screen in phase reinforced and created bright bands whereas the other which reached the screen out of phase canceled and produced dark bands as

shown in Figure 1.1. The series of bright and dark bands is called an interference fringe pattern in interferometry.

1.1.1 Theory of interference fringes

Consider a monochromatic source of light, S (Figure 1.2), which emits light of wavelength λ. The two narrow slits S_1 and S_2, separated by a small distance d which are placed close to S will receive light in phase. Therefore, the slits S_1 and S_2 act as coherent sources of light [2, 3].

The waves from S_1 and S_2 reaching a point Q on the screen travel different optical path lengths. If we draw a perpendicular line S_1R from the point S_1 on the line S_2Q, the path difference between the two waves is $S_2R = S_2Q - S_1Q$. If this path difference is an integer multiple of the wavelength of the light, the two waves will reach Q in phase. Therefore, these waves interfere constructively and create a bright band there. But if the path difference is an odd integer multiple of a half-wavelength of the light, the two waves will reach Q out of phase and hence they cancel, producing a dark band.

Using trigonometry, from right triangle S_1RS_2, the path difference

$$S_2R = d\sin\theta. \tag{1.1}$$

For a constructive interference,

$$d\sin\theta = n\lambda, \tag{1.2}$$

where n is an integer. For a destructive interference,

$$d\sin\theta = (2n+1)\frac{\lambda}{2}, \tag{1.3}$$

where n is an integer. If the distance OP between the slits and the screen is D,

$$PQ = D\tan\theta, \tag{1.4}$$

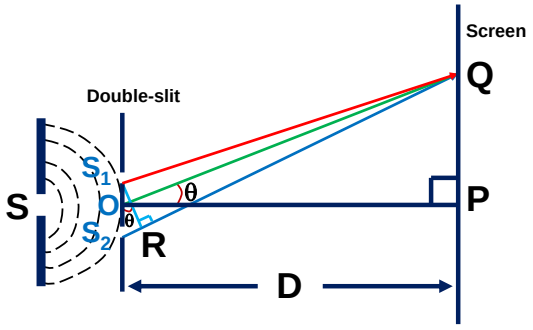

Figure 1.2 Formation of interference fringes

which gives the position of a bright or a dark fringe on the screen with respect to its center, depending upon the path difference between the waves (Eq. 1.1). Using small angle approximation in Eqs. (1.2) and (1.4), the position of a bright fringe and hence the fringe width, β of the interference fringes can be obtained in terms of experimentally measurable parameters as

$$\beta = \frac{\lambda D}{d}. \tag{1.5}$$

It can be seen from Eq. (1.5) that the interference fringes will be wider for the light of longer wavelength, smaller slit separation, and larger slit-to-screen distance.

1.2 Optical interferometry

Young's simple and elegant experiment on interference of light waves opened up a new branch of physics : optical interferometry. In a typical optical interferometer, a light beam is split much like in a double-slit, resulting in two coherent light sources, the split beams are allowed to evolve along different paths, and then finally recombined

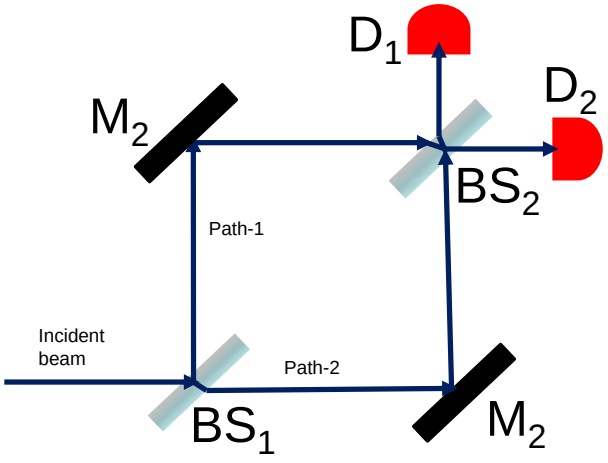

Figure 1.3 A schematic of Mach-Zehnder interferometer

to produce interference. Some common interferometer geometries are Mach-Zehnder interferometers, Michelson interferometers, and Sagnac interferometers.

In Mach-Zehnder interferometers, the splitting of the original optical beam and the recombination of the split beams take place at different locations as shown in Figure 1.3. The incident beam is split by the beamsplitter BS_1, the split beams then travel through different paths: Path-1 and Path-2, and the beams are reflected by the mirrors M_2. The reflected beams are finally recombined by the recombiner BS_2 and the interference signals are detected by the detectors D_1 or D_2 or both depending upon the phase difference between the two beams.

Unlike in a Mach-Zehnder interferometer, the splitting and recombination take place at the same location in a Michelson interferometer as shown in Figure 1.4. The incident beam is split by the beamsplitter BS, the split beams then travel through different paths: Path-1 and Path-2, and the beams are reflected by the mirrors M_1 and M_2. The two reflected beams are finally recombined by the same beamsplitter BS and the interference signals are detected by the detector D.

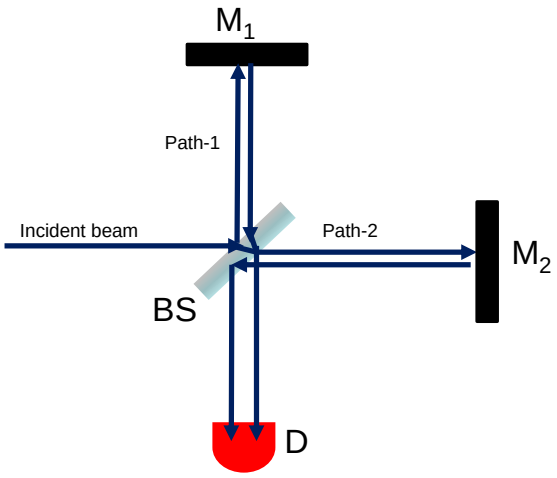

Figure 1.4 A schematic of Michelson interferometer

A third kind of interferometer which has a circular geometry as shown in Figure 1.5 is called a Sagnac interferometer. In a Sagnac interferometer, the split beams traverse different path lengths if there is a rotation of the frame of reference in which the interferometer is at rest (see Figure 1.5). This introduces a phase difference between the two beams at recombination. Therefore, a Sagnac interferometer can be used for rotation sensing. It can be shown that the phase difference at recombination is proportional to the rotation frequency, Ω and the area enclosed by the beams [4,5].

1.3 Does matter show wave nature?

Albert Einstein in 1905 gave the theory of photoelectric effect, which was based on Planck's quantum theory of radiation. According to Einstein's theory, light shows particle-like behavior. A light particle or a quantum of light is called a photon. Einstein's discovery of the law of the photoelectric effect was recognized by the 1921 Nobel Prize in Physics. Since light shows both particle-like as well as wave-like

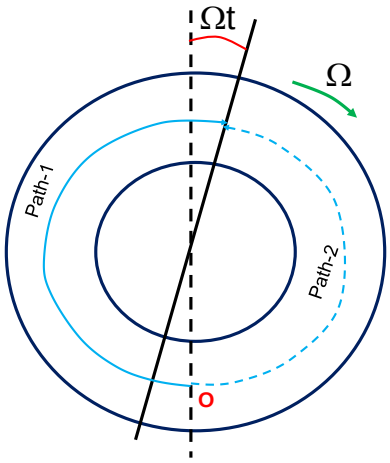

Figure 1.5 A schematic of Sagnac interferometer

behavior, why would matter not show the wave-like behavior? Intrigued by this question, Louis de Broglie in 1924 proposed in his PhD thesis that matter should show wave-like behavior. The wavelength of the matter waves, popularly known as de Broglie waves is given by $\lambda = h/(mv)$, where m is mass of a particle moving with speed v and $h = 6.63 \times 10^{-34}$ Js is the Planck's constant. The de Broglie hypothesis was verified by Davisson and Germer's experiment on electron diffraction which established the dual nature of matter. Clinton Davisson and Lester Germer in 1927 demonstrated that an electron beam passed through a double-slit arrangement produced a diffraction pattern, similar to that of Young's double-slit experiment with light. This was the first observation of matter wave interference.

1.4 Matter wave interferometry

1.4.1 Neutron interferometry

The matter wave interferometry started with the electron beams after Davisson and Germer's experiment established the wave nature of matter through the electron interference experiment. Since electrons are charged particle, the electron beams diverge laterally by Coulomb repulsion. This introduces a limitation in interferometry with electron beams [6, 7]. The discovery of neutrons in 1932 by Sir James Chadwick [8] provided a new and potentially strong candidate for matter wave interferometry because, unlike electrons, neutrons are chargeless and they are not affected by electric field. The first neutron interferometers were developed in the 1970s [9], after about 40 years of the discovery of neutrons.

1.4.2 Atom interferometry

Atom interferometry using the internal states of thermal atoms was first employed in atomic clocks by Norman Ramsey in 1950s [10]. The first successful atom interferometers of Young's double-slit type with thermal atoms were demonstrated in 1991 [11, 12]. The developement of laser cooling techniques in 1980s [13] helped to create cold atoms which made atom interferometry feasible. Atom interferometers were made by using atomic fountains with cold atoms and used to measure the acceleration due to gravity [14]. In atom interferoemters which use atomic fountains, the cold atoms are projected vertically up and manipulated by laser pulses. These free space interferometers require a large space and therefore, they are not easily portable. After the experimental realization of Bose-Einstein condensate (BEC) in 1995, there is an ultracold atomic source available to perform atom interferometry which can be conveniently controlled and manipulated by laser pulses on small atomic chips. The

BEC-based guided-wave atom interferometers confined on atom chips can be small and portable compared to large free space atom interferometers [15].

1.5 Bose-Einstein condensate

1.5.1 A brief history

Satyendra Nath Bose developed a statistics in 1920s to describe the quanta of light [16]. Einstein applied the statistics developed by Bose to a gas of noninteracting atoms and predicted that all atoms go to the same quantum state below certain temperature, called the critical or transition temperature. This state of matter was called a condensate, which later became popular as a Bose-Einstein condensate (BEC). Thus the phenomenon of Bose-Einstein condensation was predicted in 1920s. But, because of the lack of technology to cool atoms down to a very low temperature, the world had to wait for about 70 years to realize a BEC experimentally. Using the cooling techniques developed in the 1980s, the BEC was first experimentally realized in 1995 from ^{87}Rb atoms at University of Colorado [17], ^{23}Na atoms at MIT [18], and ^{7}Li atoms at Rice University [19]. Eric Cornell, Carl Wieman, and Wolfgang Ketterle were awarded the 2001 Physics Nobel Prize for the achievement of Bose-Einstein condensation in dilute alkali atoms, and for early fundamental studies of the properties of the condensates.

In a BEC, the atoms are in the same quantum state, with a very narrow velocity distribution as shown in Figure 1.6. The figure shows the velocity distribution data of an atomic BEC. The left frame of the figure corresponds to a gas at a temperature just above condensation, the center frame shows just after the appearance of the condensate, and the right frame shows after further evaporation which leaves a sample of nearly pure condensate [16].

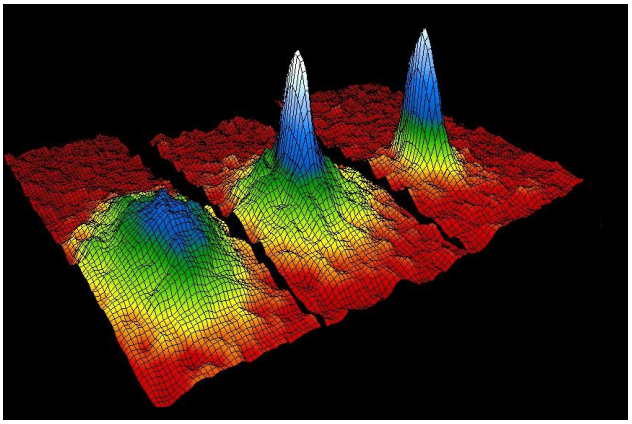

Figure 1.6 Velocity distribution in a BEC
(Source : http://jila.colorado.edu/bec/)

1.5.2 Transition temperature and condensate fraction

In this section, a brief derivation of the transition temperature for a Bose-Einstein condensation and the condensate fraction is presented. The details of the derivation can be found in references [16, 20–22].

The transition temperature T_C is defined as the highest temperature at which the macroscopic occupation of the lowest-energy state appears [20]. For a sufficiently large number N of bosonic atoms, the number of atoms in the excited states, N_e is given by

$$N_e = \int_0^\infty d\epsilon g(\epsilon) f(\epsilon), \tag{1.6}$$

where $g(\epsilon) = C_\alpha \epsilon^{\alpha-1}$ is the density of states, with C_α being a constant, and it depends upon the form of the confining potential. For example, for a three-dimensional simple harmonic oscillator, with a potential, $V(\mathbf{r}) = (m/2)(\omega_x^2 x^2 + \omega_y^2 y^2 + \omega_z^2 z^2)$, $\alpha = 3$, and

$$C_3 = \frac{1}{2\hbar^3 \omega_x \omega_y \omega_z}, \tag{1.7}$$

where ω_x, ω_y and ω_z are the angular frequencies of the three-dimensional simple harmonic oscillator potential and $\hbar = 1.055 \times 10^{-34}$ Js is the reduced Planck's constant. The function $f(\epsilon)$ in Eq. (1.6) is the Bose distribution function for the mean occupation number of the single particle state i given by

$$f(\epsilon_i) = \frac{1}{[\exp{(\epsilon_i - \mu)/k_B T}] - 1}. \tag{1.8}$$

In Eq. (1.8), μ is the chemical potential of bosonic gas, ϵ_i is the energy of the i^{th} state, T is the temperature, and $k_B = 1.38 \times 10^{-23}$J/K is the Boltzmann's constant. The number of atoms in the excited states (Eq. 1.6) achieves the greatest value for $\mu = 0$, and the transition temperature T_C is determined by the condition that the total number of particles can be accommodated in the excited states:

$$N = N_e(T_C, \mu = 0) = \int_0^\infty d\epsilon \frac{g(\epsilon)}{[\exp(\epsilon/k_B T_C)] - 1}, \tag{1.9}$$

Substituting $x = \epsilon/(k_B T_C)$ and using the standard integral,

$$\int_0^\infty dx \frac{x^{\alpha-1}}{e^x - 1} = \Gamma(\alpha)\zeta(\alpha), \tag{1.10}$$

Eq. (1.9) becomes

$$N = C_\alpha \Gamma(\alpha)\zeta(\alpha)(k_B T_C)^\alpha. \tag{1.11}$$

In Eq. (1.11), $\Gamma(\alpha) = \int dx x^{\alpha-1} e^{-x}$ is the gamma function and $\zeta(\alpha) = \sum_{n=1}^{\infty} n^{-\alpha}$ is the Riemann zeta function. Substituting C_3 (from Eq. 1.7), $\Gamma(3) = 2$, $\zeta(3) = 1.202$ [20] into Eq. (1.11), the transition temperature in a harmonic trap,

$$T_C \approx \frac{0.94\hbar\bar{\omega}}{k_B} N^{1/3}, \tag{1.12}$$

where $\bar{\omega} = (\omega_x \omega_y \omega_z)^{1/3}$ is the geometric average of the three harmonic oscillator frequencies. The typical experimental values of the trapping frequencies for an Ioffe

trap to produce a BEC are $\omega_x = \omega_y = 2\pi \times 250$ Hz and $\omega_z = 2\pi \times 16$ Hz [5]. For an atomic sodium BEC with $N = 4 \times 10^6$ atoms, Eq. (1.12) then gives $T_C = 760$ nK.

At temperature $T < T_C$, the number of particles N_e in the excited states is given by (Eq. 1.6) with $\mu = 0$. For $\alpha > 1$, the integral converges giving,

$$N_e \approx \left(\frac{k_B T}{0.94\hbar\bar{\omega}}\right)^3, \tag{1.13}$$

for C_3 given by Eq. (1.7), $\Gamma(3) = 2$ and $\zeta(3) = 1.202$. This result (Eq. 1.13) does not depend upon the total number of particles. The number of atoms in the excited state as a fraction of the total number is then obtained from Eqs. (1.12) and (1.13),

$$\frac{N_e}{N} = \left(\frac{T}{T_C}\right)^3. \tag{1.14}$$

The number of atoms in the condensate is therefore given by,

$$N_0(T) = N - N_e(T) = N\left[1 - \left(\frac{T}{T_C}\right)^3\right], \tag{1.15}$$

which gives the condensate fraction in a three-dimensional harmonic oscillator trap as,

$$\frac{N_0}{N} = 1 - \left(\frac{T}{T_C}\right)^3. \tag{1.16}$$

For the particles confined in a three-dimensional box potential, we get the historically well-known expression for the condensate fraction [16, 20, 23] as

$$\frac{N_0}{N} = 1 - \left(\frac{T}{T_C}\right)^{3/2}. \tag{1.17}$$

The BEC transition temperature is very low, in the range of some microkelvins to nanokelvins. The condensate fraction observed in a three-dimensional harmonic oscillator trap at University of Colorado, when the first BEC was observed, was at a temperature 170 nanokelvin [17].

1.5.3 The condensate wave function

The wave function of a Bose-Einstein condensate is given by

$$\psi(\mathbf{r},t) = \sqrt{n(\mathbf{r},t)}e^{i\phi(\mathbf{r},t)}, \tag{1.18}$$

where $n(\mathbf{r},t) = |\psi(\mathbf{r},t)|^2$ is the density of the condensate [16,21]. The quantity $\phi(\mathbf{r},t)$ in Eq. (1.18) is the phase and this corresponds to assuming the occurrence of a broken gauge symmetry in the many-body system [16, 21].

1.5.4 BEC and superfluidity

A superfluid flows frictionlessly through narrow channels [24]. One of the characteristic properties of a superfluid flow is the apperance of quantized vortices [25]. Superfluidity is one of the most spectacular consequences of Bose-Einstein condensation [21]. For a simple wave function given by Eq. (1.18), it can be shown that the velocity of a condensate,

$$\mathbf{v}_s = \frac{\hbar}{m}\nabla\phi. \tag{1.19}$$

Since the curl of the velocity $\mathbf{v}_s$ vanishes, this shows that the condensate velocity field is irrotational. It can be shown from Eq. (1.19) that the circulation,

$$\kappa = \oint \mathbf{v}_s \cdot d\mathbf{l} = n\frac{h}{m}, \tag{1.20}$$

where n is an integer, and m is the atomic mass. Eq. (1.20) shows that the circulation in a superfluid is quantized, with the quantum of circulation as (h/m) [24]. Quantized vortices in superfluids were first predicted independently by Onsager (1949) and Feynman (1955) and hence Eq. (1.20) is called Onsager-Feynman quantization condition [22]. It has been shown both theoretically [21, 22, 26, 27] and experimentally that Bose-Einstein condensate in dilute alkali gases shows superfluidity and supports the formation of quantized vortices [28, 29] as in superfluid liquid helium [25].

1.5.5 Gross-Pitaevskii equation

This dissertation analyzes BEC-based atom interferometers in the framework of mean-field approximation by Gross-Pitaevskii equation. In this section, a brief derivation of the time dependent Gross-Pitaevskii equation is presented. More details of the derivation can be found in [16, 21, 22] , and the references therein.

Consider a system with N interacting bosons confined by an external potential V_{ext}. The second quantized many-body Hamiltonian for the system,

$$\hat{H} = \int d^3\mathbf{r}\hat{\Psi}^\dagger(\mathbf{r},t)H_0\hat{\Psi}(\mathbf{r},t) + \frac{1}{2}\int d^3\mathbf{r}\int d^3\mathbf{r}'\hat{\Psi}^\dagger(\mathbf{r}',t)V_{int}(\mathbf{r}'-\mathbf{r})\hat{\Psi}(\mathbf{r}',t), \quad (1.21)$$

where

$$H_0 = -\frac{\hbar^2}{2m}\nabla^2 + V_{ext}, \quad (1.22)$$

is the single particle Hamiltonian. The second term in the right hand side of Eq. (1.21) arises from the atom-atom interactions. The field operators $\hat{\Psi}^\dagger(\mathbf{r}',t)$ and $\hat{\Psi}(\mathbf{r}',t)$ are the creation and annihilation field operators respectively which satisfy the following commutation relations:

$$\begin{aligned}\left[\hat{\Psi}(\mathbf{r},t),\hat{\Psi}^\dagger(\mathbf{r}',t)\right] &= \delta(\mathbf{r},\mathbf{r}'),\\ \left[\hat{\Psi}(\mathbf{r},t),\hat{\Psi}(\mathbf{r}',t)\right] &= 0.\end{aligned} \quad (1.23)$$

The time evolution of the field operator $\hat{\Psi}(\mathbf{r},t)$ is given by the Heisenberg equation:

$$i\hbar\frac{\partial\hat{\Psi}(\mathbf{r},t)}{\partial t} = \left[\hat{\Psi}(\mathbf{r},t),\hat{H}\right]. \quad (1.24)$$

Using the Hamiltonian from Eq. (1.21) and the commutation relations for the field operators from Eq. (1.23), the evolution equation for the operator (Eq. 1.24) takes the following form :

$$i\hbar\frac{\partial\hat{\Psi}(\mathbf{r},t)}{\partial t} = \left[-\frac{\hbar^2}{2m}\nabla^2 + V_{ext}(\mathbf{r},t)\right]\hat{\Psi}(\mathbf{r},t) + \int d^3\mathbf{r}'\hat{\Psi}^\dagger(\mathbf{r}',t)V_{int}(\mathbf{r}'-\mathbf{r})\hat{\Psi}(\mathbf{r}',t)\hat{\Psi}(\mathbf{r},t). \quad (1.25)$$

For a sufficiently dilute gas, atom-atom interactions are dominated by low-energy, two-body s - wave collisions. Therefore, the interaction potential is given by

$$V_{int}(\mathbf{r}' - \mathbf{r}) = g\delta(\mathbf{r}' - \mathbf{r}), \tag{1.26}$$

with $g = 4\pi\hbar^2 a_s/m$, m and a_s being the atomic mass the s - wave scattering length respectively. Using Bogoliubov prescription, we decompose the field operator as

$$\hat{\Psi}(\mathbf{r}', t) = \psi(\mathbf{r}', t) + \delta\hat{\Psi}(\mathbf{r}', t), \tag{1.27}$$

where $\psi(\mathbf{r}', t) \equiv \langle\hat{\Psi}(\mathbf{r}', t)\rangle$ is the macroscopically-populated mean field term and it is called the *wave function of the condensate*(see Section 1.5.3). Its modulus fixes the density of the condensate through

$$n(\mathbf{r}', t) = |\psi(\mathbf{r}', t)|^2. \tag{1.28}$$

The term $\delta\hat{\Psi}(\mathbf{r}, t)$ in Eq. (1.27) is the thermal and quantum depletion of the condensate and it is small for sufficiently weakly-interacting condensate at temperatures much less than the transition temperature for condensation.

Substituting for $V_{int}(\mathbf{r}' - \mathbf{r})$ from Eq. (1.26) and $\hat{\Psi}(\mathbf{r}', t)$ from Eq. (1.27) into Eq. (1.25), and retaining only the leading order terms in $\psi(\mathbf{r}, t)$ gives,

$$i\hbar\frac{\partial\psi(\mathbf{r}, t)}{\partial t} = \left[-\frac{\hbar^2}{2m}\nabla^2 + V_{ext}(\vec{r}, t) + g|\psi(\mathbf{r}, t)|^2\right]\psi(\mathbf{r}, t). \tag{1.29}$$

The Eq. (1.29) is the time dependent Gross - Pitaevskii equation. It was first derived independently by E. P. Gross and L. P. Pitaevskii in 1961 [16].

1.5.6 Thomas-Fermi approximation

To describe the ground state of a condensate, we separate the condensate wave function $\psi(\mathbf{r}, t)$ into spatial and temporal part as follows:

$$\psi(\mathbf{r}, t) = \psi(\mathbf{r})e^{-i\mu t/\hbar} \tag{1.30}$$

where μ is the chemical potential and $\psi(\mathbf{r})$ is real and normalized to the total number of particles :

$$\int d^3\mathbf{r}|\psi(\mathbf{r})|^2 = N \tag{1.31}$$

Substituting $\psi(\mathbf{r},t)$ from Eq. (1.30) into Eq. (1.29) gives

$$\left[-\frac{\hbar^2}{2m}\nabla^2 + V_{ext}(\mathbf{r}) + g|\psi(\mathbf{r})|^2\right]\psi(\mathbf{r}) = \mu\psi(\mathbf{r}), \tag{1.32}$$

which is the time-independent Gross-Pitaevskii equation.

For a sufficiently large condensate, the interaction energy term from the atom-atom interactions is much larger than the kinetic energy term. In this situation, we can neglect the kinetic energy term from the left hand side of Eq. (1.32) to get

$$\left[V_{ext}(\mathbf{r}) + g|\psi(\mathbf{r})|^2\right]\psi(\mathbf{r}) = \mu\psi(\mathbf{r}). \tag{1.33}$$

This is called the Thomas-Fermi approximation [5,16,20,21]. The solution to Eq. (1.33) is

$$n(\mathbf{r}) = |\psi(\mathbf{r})|^2 = \frac{\mu - V_{ext}(\mathbf{r})}{g} \tag{1.34}$$

in the region where the right hand side is positive and $\psi(\mathbf{r}) = 0$ outside this region. The boundary of the cloud is given by

$$V_{ext}(\mathbf{r}) = \mu \tag{1.35}$$

The physics of Eq. (1.33) is that the energy to add a particle at any point in the cloud is the same everywhere. This energy is given by the sum of the external potential $V_{ext}(\mathbf{r})$ and the interaction contribution $n(\mathbf{r})g$ which is the chemical potential of a uniform gas having density equal to the local density $n(\mathbf{r})$ [20].

1.5.7 BEC on chip

The development of magnetic microtraps [30] has made it possible for the preparation and control of BEC using an atom chip [31–33]. Farkas et al. [34] have recently developed a compact, transportable, microchip-based system for high repetition rate production of Bose-Einstein condensates. Their on-chip BEC system occupies a volume of 0.4 m^3 and the entire process of preparing and imaging a BEC takes place at the rate of 0.3 Hz, which means that one complete cycle is carried out in about 3 seconds. This time includes loading atoms from a vapor into a magneto-optical trap (MOT), transporting the atoms up to the atom chip, evaporative cooling, and imaging. Horikoshi et al. [33] also prepared a BEC at the same rate but the total number of atoms in their BEC was 3×10^3, where as a BEC prepared by Farkas et al. [34] was bigger with the number of atoms of 1.9×10^4.

1.5.8 BEC-based atom interferometry

Atom interferometers using cold atoms or Bose-Einstein condensates (BECs) can have very high sensitivities in comparison to their optical counterparts [31], and can find potential applications in field-sensing and precision measurements [35]. Atom interferometers can be more versatile than the optical ones and have been used to measure acceleration [14], rotations [36], and dynamic polarizability of atoms [37]. The laser cooling techniques of neutral atoms developed in the 1980s [13] opened up the applications of ultra cold atoms in atom interferometry.

After the experimental realizations of BECs in dilute atomic gases in the mid-1990s [17–19], the horizon of atom interferometry has broadened. The atoms in BECs have a very narrow momentum distribution and hence can be controlled and manipulated more easily than the thermal atoms by using light waves. Moreover, all atoms in

BECs are in the same quantum state and hence BECs are excellent coherent sources of matter waves. The interference of two independent condensates was first reported in [38], in which two separate condensates were prepared in a double-well potential and allowed to interfere by switching off the potential and letting the condensates expand. Shin et al. [39] showed trapped atom interferometry with a condensate prepared in an optical single-well potential and then coherently split into two by deforming the single-well into a double-well potential. This, as well as several other experiments [31,32,40,41] on BEC-based atom interferometry, shows that condensates are good candidates for interferometric applications. BEC-based atom interferometers in Michelson geometry [31, 42] and in Mach-Zehnder geometry [33, 43] were realized recently.

The basic steps of guided-wave atom interferometry are the following [15]: an atomic wave packet is split into two in a trap or a wave guide, the split wave packets are sent down two different paths, and recombined at the end of the interferometric cycle. For example, in a single-reflection atom Michelson interferometer, a BEC in a zero momentum state ψ_0 is split at time $\tau = 0$ by a laser standing wave into two harmonics ψ_+ and ψ_- [31, 44, 45]. The atoms in the ψ_+ harmonic absorb a photon from a laser beam with the momentum $\hbar k$ and re-emit into the beam with the momentum $-\hbar k$ (with k being the wave number of the laser,) thus acquiring velocity $v_0 = 2\hbar k/M$, where M is the atomic mass. Similarly, an atom in the ψ_- harmonic acquires velocity $-v_0 = -2\hbar k/M$. At time $\tau = T/2$, where T is the interferometric cycle time, a reflection pulse is applied to reverse the momenta of the harmonics. At time $\tau = T$, the two harmonics are subject to the action of a recombination pulse. After recombination, in general, the atoms populate all three harmonics ψ_0 and $\psi_\pm$. The number of atoms in each harmonic depends on the relative phase acquired during the interferometric cycle and can be used to deduce this phase.

1.6 Outline of the thesis

We analyze a BEC-based free oscillation atom Michelson interferometer in Chapter 2. The analysis is done in the framework of mean-field approximation by one-dimensional Gross-Pitaevskii equation. In a free oscillation atom interferometer, a BEC in a harmonic oscillator potential is split by laser pulses and the split clouds are allowed to evolve freely. Those clouds turn around at their classical turning points, and undergo free oscillations before they are finally recombined at the end of an interferometric cycle. Because of the nonlinearity due to atom-atom interactions in a BEC, the motion of a split condensate in harmonic oscillator trap is complicated. For example, the size of the split clouds oscilllates at a frequency different from the trap frequency. The phases have their own dynamics. We study the dynamics of the split condensates in the interferometer and investigate the effect of trap frequencies and nonlinearity on the contrast of the interferometric fringes. We derive the theoretical limit of performance of the interferometer in terms of experimental parameters: the trap frequencies, number of atoms in the condensate, and the velocity of the split clouds imparted by the splitting laser pulses. Finally, we compare our predictions with the recent experimental results.

In Chapter 3, the dynamics of a split-condensate in BEC-based single and double reflection atom Michelson interferometers is studied. Unlike in a free oscillation interferometer, multiple reflection pulses are applied to return the split clouds in reflection type interferometers. We derive expressions for the difference of velocity of a split cloud at recombination and its initial velocity in each of the single and double reflection interferometers. Since the velocity difference does the major contribution on accumulation of the spatial relative phase between the split clouds and hence on the loss of contrast [46], we compare this quantity in these interferometers to that

of a free oscillation interferometer. We also compare our results with the analogous results in [46, 47] obtained by completely different technique.

In Chapter 4, we give our conclusions on the work of this thesis and outline a future direction. We point out the requirement of higher dimensional analytical model for a complete description of a free oscillation interferometer in the cases when the split clouds oscillate on a plane.

The Appendix A contains a reprint of the published paper on free oscillation atom Michelson interferometer.

Chapter 2

A free oscillation atom interferometer

'An equation is for eternity.' - Albert Einstein

2.1 Introduction

In this chapter, we theoretically analyze a Bose-Einstein condensate (BEC)-based free oscillation atom Michelson interferometer in a weakly confining magnetic trap. A free oscillation atom interferometer in Michelson geometry [40, 48] and in Mach-Zehnder geometry [33] were experimentally realized recently. In a free oscillation atom Michelson interferometer, a BEC wave packet ψ at the center of a weakly confining harmonic trap is split into two harmonics ψ_+ and ψ_- by a laser pulse, which in turn consists of two short subpulses. The ψ_+ harmonic moves to the right with a speed $v = 2\hbar k/M$ and ψ_- harmonic moves to the left with the same speed. Here k is the wave number of the splitting laser and M is the atomic mass in the condensate. The harmonics turn back under the influence of the trapping potential at their classical

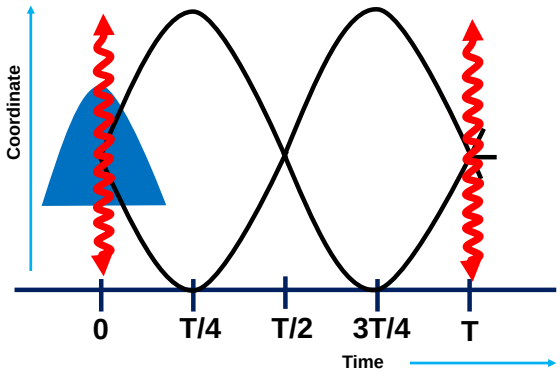

Figure 2.1 A schematic of a free oscillation interferometer.

turning points. The split harmonics perform a full cycle oscillation in the trap so that the interferometric time, $T = mT_0$, where $T_0 = 2\pi\omega^{-1}$ is the longitudinal trap period and m is an integer. They are finally recombined at the end of m cycles with laser pulses which are identical to the splitting pulses.

A schematic diagram of the interferometer is shown in Figure 2.1. The sinusoidal curves going from left to right show the trajectories of the split condensates and the vertical wavy lines represent the splitting and recombination laser pulses.

There are two major factors which degrade the contrast of the interferometer fringes in this type of interferometer. (1) The split condensates have finite size and they oscillate in a harmonic trap. This causes an unequal phase distribution across each harmonic which results into spatial phase gradient across them. (2) Since a BEC is a degenerate gas, there is a repulsive force due to the atom-atom interactions in the condensate. For the sake of definiteness, we consider a condensate of ^{87}Rb atoms which have positive s-wave scattering length. The nonlinearity in these atoms is positive. The repulsive nonlinearity imparts a momentum to the atoms when the split clouds are overlapping [49]. The contribution in the velocities caused by nonlinear

atomic interactions causes an adverse effect in interferometry because the recombination pulse can not compensate the velocities of the harmonics at the recombination. This causes an accumulation of a spatially dependent phase across the clouds [45,50]. Right after the splitting pulse is applied, the split clouds move in opposite directions and the different parts of the clouds interact for different lengths of time. The front or the leading edges of the harmonics interact for the least amount of time whereas the back or the trailing edges of the harmonics interact until their complete separation takes place. This also causes a coordinate dependent phase to develop across the harmonics, which degrades the contrast of the interference fringes [40].

We study theoretically the dynamics of the split condensates in a free oscillation atom Michelson interferometer, derive an expression for the contrast of the interferometric fringes, and obtain the fundamental limit of performance of the interferometer in the parameter space.

2.2 Analytical model

The evolution of a BEC in a weakly-confining parabolic potential of longitudinal frequency ω is described in the framework of the mean-field approximation by the dimensionless Gross-Pitaevskii equation (GPE):

$$i\frac{\partial}{\partial\tau}\psi(X,\tau) = \left[-\frac{\epsilon}{2}\frac{\partial^2}{\partial X^2} + \frac{1}{2\epsilon}X^2 + g_{1D}|\psi(X,\tau)|^2\right]\psi(X,\tau). \tag{2.1}$$

This equation can be obtained by projecting the three-dimensional GPE onto the strongly confining transverse mode of the wave guide as in [45]. The axial coordinate x is normalized to the initial longitudinal radius L_0 of the condensate: $X = x/L_0$. The dimensionless time τ is given by the relation $\tau = \omega t$, where ω is the longitudinal frequency of the weakly-confining potential and t is the dimensional time. The

strength of interatomic interactions is described by the parameter

$$g_{1D} = 2\omega_\perp a_s N/(\omega L_0) \tag{2.2}$$

where a_s is the s-wave scattering length, N is the total number of atoms in the condensate and $\omega_\perp$ is the trapping angular frequency in the tightly confined transverse dimensions. Finally, $\epsilon = (a_0/L_0)^2$, where $a_0 = \sqrt{\hbar/(M\omega)}$ is the oscillator length along the longitudinal dimension. The wave function ψ has been normalized to 1.

The initial equilibrium size of the condensate in the Thomas-Fermi approximation [21] is given by:

$$L_0 = \left(\frac{3\hbar\omega_\perp a_s N}{M\omega^2}\right)^{1/3}. \tag{2.3}$$

2.3 Splitting of the condensate

2.3.1 Wave function of split condensate

A laser pulse consisting of a sequence of two subpulses is applied for a short period of time to split the intial atomic wave packet. The wave function ψ of the condensate after the splitting pulse is a superposition of two harmonics $\psi_\pm$:

$$\psi = \frac{1}{\sqrt{2}}(\psi_+ + \psi_-), \tag{2.4}$$

where ψ_+ and ψ_- are the wave functions of the initially right-moving and left-moving clouds respectively. The wave functions $\psi_\pm$ are defined as:

$$\psi_\pm = \sqrt{n_\pm}\exp(i\phi_\pm), \tag{2.5}$$

and they have been normalized to 1. In Eq. (2.5), $\phi_\pm$ are the phases of the split clouds with the wave functions $\psi_\pm$. The splitting pulse acts on the condensate for a very short period of time. Therefore, the density profile (shape of the clouds) remains unchanged during splitting.

2.3.2 The density and phase

The density of the split condensate is given by

$$n_{\pm}(x \mp x_0) = \frac{3}{4L}\left[1 - \left(\frac{x \mp x_0}{L}\right)^2\right], \tag{2.6}$$

where $\pm x_0(t)$ are the coordinates of the center of mass (CM) of the split clouds and $L(t)$ is the radius of each cloud. The radius of the cloud is the half width of the Thomas-Fermi profile along the weakly trapped dimension. The phase is defined as

$$\phi_{\pm}(x \mp x_0) = \phi_{0,\pm} \pm \frac{M}{\hbar} v(x \mp x_0) + \frac{g}{2L^2}(x \mp x_0)^2 \pm \frac{s}{6L^3}(x \mp x_0)^3, \tag{2.7}$$

where $\phi_0(t)$, $v(t)$, $g(t)$, and $s(t)$ are the phase due to the environment, the speed of a split cloud, the quadratic, and the cubic phases respectively. The wave functions $\psi_{\pm}(x \mp x_0)$ have been normalized to 1, which means that $\int_a^b n_{\pm}(x \mp x_0) = 1$. The integration limits $a = \pm x_0 - L$ and $b = \pm x_0 + L$ are the edges of the clouds along the longitudinal dimension.

To make the analysis of the interferometer simpler, we introduce normalized variables to express the density and phase in dimensionless form as follows: $X = x/L_0$, $X_0(\tau) = x_0(t)/L_0$, $V(\tau) = v(t)/(\omega L_0)$, $G(\tau) = \epsilon g(t)$, $S(\tau) = \epsilon s(t)$, where $\epsilon = (\hbar/M\omega)/L_0^2 = (a_0/L_0)^2 << 1$, $a_0 = \sqrt{\hbar/(M\omega)}$ being the oscillator length. The dimensionless time τ is defined by the relation, $\omega t = \tau$, where t is the dimensional time. In dimensionless variables, the densities $n_{\pm}$ and the phases $\phi_{\pm}$ of the harmonics ψ_+ and ψ_- are as follows:

$$\begin{aligned} n_{\pm} &= \frac{3}{4R}\left[1 - \left(\frac{X \mp X_0}{R}\right)^2\right], \\ \phi_{\pm} &= (\phi_0)_{\pm} + \frac{1}{\epsilon}\left[\pm V(X \mp X_0) + \frac{G}{2}\left(\frac{X \mp X_0}{R}\right)^2 \pm \frac{S}{6}\left(\frac{X \mp X_0}{R}\right)^3\right]. \end{aligned} \tag{2.8}$$

In Eq. (2.8), $\pm X_0(\tau)$ are the positions of the centers of mass of the two harmonics and $R(\tau) = L/L_0$ is their dimensionless radius. As described above, the harmonics'

shape and position immediately after splitting are equal to those of the initial BEC at rest, i.e., $X_0(0) = 0$ and $R(0) = 1$.

2.3.3 How do various phase terms appear?

In the expression for the total phase of the split BEC (the second equation of the Eq. (2.8)), the term $(\phi_0)_\pm$ are the phases accrued by the harmonics from the environment. The terms $\pm V(X \mp X_0)$ are due to the motion of the two harmonics. The parameter $V(\tau)$ is the normalized speed $v(t)$ of the harmonics, i.e., $V(\tau) = v(t)/(\omega L_0)$ with the initial value $V(0) = V_0 = v_0/(\omega L_0)$. The quadratic term proportional to $G(\tau)$ appears because of dispersion of the harmonics. The cubic term proportional to $S(\tau)$ is due to atom-atom interactions in the condensate. The quadratic and cubic phases are initially zero,i.e., $G(0) = S(0) = 0$, and evolve with time when the harmonics start propagating.

2.4 Dynamical evolution of the split condensate

2.4.1 Hamiltonian of the split condensate

The Hamiltonians of the BEC clouds after the splitting is given by

$$H_\pm = \frac{p^2}{2m} + \frac{1}{2}m\omega^2 x^2 + \frac{1}{2}g_{1D}(n_\pm + 2n_\mp), \tag{2.9}$$

where $n_\pm$ are the densities of the two clouds and are given by Eq. (2.6) and $g_{1D} = (U_0 N)/(2\pi a_\perp^2) = 2\hbar N a_s \omega_\perp$ is the strength of nonlinearity in one dimensional model. In dimensionless form, Eq. (2.9) can be written as

$$H_\pm = \frac{\epsilon}{2}P^2 + \frac{1}{2\epsilon}X^2 + \frac{1}{2}g_{1D}(n_\pm + 2n_\mp), \tag{2.10}$$

where $\epsilon = (a_0/L_0)^2$, $P = p/(m\omega L_0)$ is the dimensionless momentum , and the g_{1D} is the dimensionless nonlinearity parameter (Eq. 2.2).

2.4.2 Expectation values of dynamical quantities

We derive the equations of motion for the various parameters of the split condensate by evaluating the quantum mechanical expectation values of the dynamical quantities. The expectation value of a quantity, x with respect to the wave function, ψ is defined as

$$\langle x\rangle = \langle\psi|x|\psi\rangle = \int_{-\infty}^{+\infty} dx\psi^* x\psi. \tag{2.11}$$

In the following, we will find the expectation values of all the dynamical quantities with respect to the wave function ψ_+. For the sake of clarity in notation, we have dropped the + sign from the ψ_+, and hereafter ψ_+ is simply written as ψ.

The expectation value of the coordinate x,

$$\langle x\rangle = \langle\psi|x|\psi\rangle = \int_{-\infty}^{+\infty} dx\psi^* x\psi = x_0, \tag{2.12}$$

and that of momentum p,

$$\langle p\rangle = \langle\psi|p|\psi\rangle = -i\hbar\int_{-\infty}^{+\infty} dx\psi^*\frac{\partial}{\partial x}\psi = M\left(v + \frac{s\hbar}{10ML}\right). \tag{2.13}$$

The expectation value of x^2,

$$\langle x^2\rangle = \langle\psi|x^2|\psi\rangle = \int_{-\infty}^{+\infty} dx\psi^* x^2\psi = x_0^2 + \frac{1}{5}L^2. \tag{2.14}$$

The expectation value of p^2,

$$\begin{aligned}\langle p^2\rangle &= \langle\psi|p^2|\psi\rangle = \hbar^2\int_{-\infty}^{+\infty} dx\left|\frac{\partial\psi}{\partial x}\right|^2 \\ &= M^2\left(v + \frac{s\hbar}{10ML}\right)^2 + \frac{2}{175}\left(\frac{s\hbar}{L}\right)^2 + \frac{1}{5}\left(\frac{g\hbar}{L}\right)^2.\end{aligned} \tag{2.15}$$

The expectation value of n_-, $\langle n_-\rangle = \int dx\psi_+^* n_-\psi_+$ can be obtained by evaluating the integral from $x = -1 + |q|$ to $x = 1 - |q|$, where $q = x_0/L$. This is the integral of the overlap region of the n_+ and n_-. Therefore,

$$\langle n_-\rangle = \int_{-1+|q|}^{1-|q|} dx n_+ n_- = -\frac{3}{5L}(|q|-1)^3(q^2+3|q|+1)\theta(|q|<1), \tag{2.16}$$

where $n_\pm$ are the densities of the initially right moving (ψ_+) and left moving (ψ_-) clouds (Eq. 2.6). Putting together, the expectation values of various dynamical quantities are as follows:

$$\begin{aligned}
\langle x\rangle &= x_0, \\
\langle p\rangle &= M\left(v+\frac{s\hbar}{10ML}\right), \\
\langle x^2\rangle &= x_0^2+\frac{1}{5}L^2, \\
\langle p^2\rangle &= M^2\left(v+\frac{s\hbar}{10ML}\right)^2+\frac{2}{175}\left(\frac{s\hbar}{L}\right)^2+\frac{1}{5}\left(\frac{g\hbar}{L}\right)^2, \qquad (2.17)\\
\langle n_+\rangle &= \frac{3}{5L}, \\
\langle n_-\rangle &= -\frac{3}{5L}(|q|-1)^3(q^2+3|q|+1)\theta(|q|<1). \qquad (2.18)
\end{aligned}$$

The expectation value of n_- can be expressed in the following form:

$$\langle n_-\rangle = \frac{3}{5L}(5qf_1+f_2), \qquad (2.19)$$

where f_1 and f_2 are given by

$$\begin{aligned}
f_1(q) &= -\frac{q}{2}(|q|-1)^2(14|q|^3+28q^2-23|q|-4)\theta(|q|<1), \\
f_2(q) &= -(|q|-1)^2(6|q|^3+12|q|^2-2|q|-1)\theta(|q|<1). \qquad (2.20)
\end{aligned}$$

The parameter $q = x_0/L$ in Eq. (2.20) is the relative position of the center of mass of a harmonic. The θ-function in Eq. (2.20) is equal to one if its argument is a logical true and zero if it is a logical false. These functions arise because of the interatomic interactions between the two harmonics.

2.4.3 Equations of motion

We derive the equations of motion to different parameters from the expectation values of various dynamical quantities evaluated in Section 2.4.2. The equation of motion

for a quantity, A is given by

$$\frac{d}{dt}\langle A\rangle = \frac{i}{\hbar}\langle\psi|[H,A]|\psi\rangle, \tag{2.21}$$

where $[H,A] = (HA - AH)$ is a commutation relation of A with the Hamiltonian H of the system:

$$H = \frac{p^2}{2M} + W(x) = \frac{p^2}{2M} + V(x) + g_{1D}(n_+ + 2n_-). \tag{2.22}$$

The following relations are required in deriving the equations of motion:

$$\begin{aligned} [x, W(x)] &= 0, \\ [f(x), p] &= i\hbar\frac{df(x)}{dx}, \\ \left[H, p^2\right] &= i\hbar(W_x p + pW_x), \end{aligned} \tag{2.23}$$

where $W_x = dW/dx$. We derive the equations of motion for various parameters by substituting the expectation values from Eq. (2.17) to Eq. (2.21). For $A = p^2$ in Eq. (2.21), and employing, $\psi = \sqrt{n}\exp(i\phi)$ gives,

$$\frac{d}{dt}\langle p^2\rangle = -\langle(pW_x + W_x p)\rangle = -2\hbar\int dx\phi_x n W_x. \tag{2.24}$$

If A is the function of coordinates only, from the Eq. (2.21),

$$\frac{d}{dt}\langle A(x)\rangle = \frac{1}{2M}(\langle pA_x + A_x p\rangle), \tag{2.25}$$

where $A_x = dA/dx$ and for $A = x$,

$$\frac{d}{dt}\langle x\rangle = \frac{1}{M}\langle p\rangle. \tag{2.26}$$

We get the speed of the center of mass of the split cloud from the Eq. (2.26) by substituting the expectation values of x and p from Eq. (2.17):

$$\frac{dx_0}{dt} = v + \frac{s\hbar}{10ML}. \tag{2.27}$$

We can write the Eq. (2.25) as,

$$\frac{d}{dt}\langle A(x)\rangle = -i\frac{\hbar}{2M}\int_{-\infty}^{+\infty} dx\psi^*\left[\frac{\partial}{\partial x}(A_x\psi) + A_x\frac{\partial}{\partial x}\psi\right]. \tag{2.28}$$

Employing the integration by parts in the limits from $x = -\infty$ to $x = +\infty$, setting the integrated term to zero, and then substituting $\psi = \sqrt{n}\exp(i\phi)$ gives the following:

$$\begin{aligned}\frac{d}{dt}\langle A(x)\rangle &= -i\frac{\hbar}{2M}\int_{-\infty}^{+\infty} dx(\psi_x^* A_x\psi - \psi^* A_x\psi_x) \\ &= \frac{\hbar}{M}\int dx\phi_x n A_x. \end{aligned}\tag{2.29}$$

where the subscript x to a variable in the right hand side is its derivative with respect to x. In deriving the equations of motion for phases, we need the expectation value of $(xp + px)/2$ which is as follows:

$$\langle (xp+px)/2\rangle = \int_{-\infty}^{-\infty} dx\psi^*(xp+px)\psi = M\left[x_0\left(v + \frac{s\hbar}{10ML}\right) + \frac{g\hbar}{5M}\right]. \tag{2.30}$$

For $A = x^2$, the Eq. (2.29) gives,

$$\frac{d}{dt}\langle x^2\rangle = 2x_0\left(v + \frac{s\hbar}{10ML}\right) + \frac{2g\hbar}{5M}. \tag{2.31}$$

Differentiating the third of Eq. (2.17) explicitly on both sides with respect to time, substituting dx_0/dt from Eq. (2.27), and equating the result to the right hand side of the Eq. (2.31), we get the equation of motion for the size of the clouds as follows:

$$\frac{dL}{dt} = \frac{g\hbar}{ML}. \tag{2.32}$$

From the Eq. (2.21), for $A = p$,

$$\frac{d}{dt}\langle p\rangle = -\langle W_x\rangle = -M\omega^2 x_0 - \frac{1}{2}g_{1D}\langle (n_+)_x\rangle - g_{1D}\langle (n_+)_x\rangle, \tag{2.33}$$

where $\langle x\rangle = x_0$ has been used and n_x represents the spatial derivative of the density. But, since $\langle (n_+)_x\rangle = 0$, and $\langle (n_-)_x\rangle = [-3/(2L^2)]q(|q|-1)^2(|q|+2)$, using the expectation value of p,

$$\frac{d}{dt}\left(v + \frac{s\hbar}{10ML}\right) = -\omega^2 x_0 + \frac{\omega^2 L_0^3}{L^2}q(|q|-1)^2(|q|+2). \tag{2.34}$$

From the Eq. (2.21), for $A = (xp + px)/2$,

$$\frac{d}{dt}\left\langle \frac{xp+px}{2} \right\rangle = \frac{\langle p^2 \rangle}{M} + \int dx(nW + xWn_x). \tag{2.35}$$

The integrals

$$\begin{aligned}
\int dxWn_+ &= \frac{1}{2}M\omega^2\left(x_0^2 + \frac{1}{5}L^2\right) + \frac{M\omega^2 L_0^3}{5L}[1 - 2(|q|-1)^3(|q|^2+3|q|+1), \\
\int dxxWn_x &= -\frac{3}{2}M\omega^2\left(x_0^2 + \frac{1}{5}L^2\right) - \frac{M\omega^2 L_0^3}{10L} \\
&+ \frac{M\omega^2 L_0^3}{5L}[(|q|-1)^3(|q|^2+3|q|+1)].
\end{aligned} \tag{2.36}$$

On substituting the above integrated expressions for $\int dxWn_+$ and $\int dxxWn_x$ and the expression for $\langle p^2 \rangle$ from (fourth of Eq. 2.17) into Eq. (2.35) gives

$$\begin{aligned}
\frac{d}{dt}\left\langle \frac{xp+px}{2} \right\rangle &= M\left(v + \frac{s\hbar}{10ML}\right)^2 + \frac{2}{175M}\left(\frac{s\hbar}{L}\right)^2 + \frac{1}{5M}\left(\frac{g\hbar}{L}\right)^2 - M\omega^2\left(x_0^2 + \frac{L^2}{5}\right) \\
&+ \frac{M\omega^2 L_0^3}{10L}[1 - 2(|q|-1)^3(|q|^2+3|q|+1).
\end{aligned} \tag{2.37}$$

Since $W(x) = V(x) + (g_{1D}/2)(n_+ + 2n_-) = M\omega^2 x^2/2 + g_{1D}n_+/2 + g_{1D}n_-)$, the time derivative of the expectation value of p^2 can be written as

$$\frac{d}{dt}\langle p^2 \rangle = \frac{d}{dt}\langle p^2 \rangle_V + \frac{d}{dt}\langle p^2 \rangle_n, \tag{2.38}$$

where the first term in the right hand side of Eq. (2.38) shows the linear part of the potential and the second term shows the nonlinear part. Hence from the Eq. (2.24)

$$\frac{d}{dt}\langle p^2 \rangle_V = -2\hbar \int dx \phi_x n \frac{dV}{dx} = -2M^2\omega^2\left[x_0\left(v + \frac{s\hbar}{10ML}\right) + \frac{g\hbar}{5M}\right], \tag{2.39}$$

is the contribution from the V part of the potential, where $\phi_x = d\phi/dx = Mv/\hbar + (g/L^2)(x - x_0) + (s/2L^3)(x - x_0)^2$. The nonlinear contribution gives the following expression:

$$\frac{d}{dt}\langle p^2 \rangle_n = -2\hbar \int dx \phi_x n \frac{d}{dx}\left[\frac{g_{1D}}{2}(n_+ + 2n_-)\right]$$

$$
\begin{aligned}
&= \frac{M\omega^2 L_0^3}{5L^3} g\hbar + \frac{2M\omega^2 L_0^3}{L^2} vq(|q|-1)^2(|q|+2) \\
&- \frac{2M\omega^2 L_0^3}{5L^3} g\hbar(|q|-1)^2(6|q|^3+12|q|^2-2|q|-1) \\
&+ \frac{M\omega^2 L_0^3}{5L^3} s\hbar q(|q|-1)^2(8|q|^3+16|q|^2-11|q|+2). \qquad (2.40)
\end{aligned}
$$

Therefore, from Eqs. (2.38), (2.39), and (2.40),

$$
\begin{aligned}
\frac{d}{dt}\langle p^2\rangle &= -2M^2\omega^2\left[x_0\left(v+\frac{s\hbar}{10ML}\right)+\frac{g\hbar}{5M}\right] \\
&+ \frac{M\omega^2 L_0^3}{5L^3} g\hbar + \frac{2M\omega^2 L_0^3}{L^2} vq(|q|-1)^2(|q|+2) \\
&- \frac{2M\omega^2 L_0^3}{5L^3} g\hbar(|q|-1)^2(6|q|^3+12|q|^2-2|q|-1) \\
&+ \frac{M\omega^2 L_0^3}{5L^3} s\hbar q(|q|-1)^2(8|q|^3+16|q|^2-11|q|+2). \qquad (2.41)
\end{aligned}
$$

Taking the explicit time derivative of $\langle p^2\rangle$ (fourth of Eq. 2.17) and making relevant substitutions from the Eqs. (2.32) and (2.34),

$$
\begin{aligned}
\frac{d}{dt}\langle p^2\rangle &= -2M^2\omega^2 x_0 v + \frac{2M^2\omega^2 L_0^3}{L^2} vq(|q|-1)^2(|q|+2) + \frac{M\omega^2 L_0^3}{5L^3} s\hbar q(|q|-1)^2(|q|+2) \\
&- \frac{M\omega^2 x_0}{5L} s\hbar + \frac{4s\hbar^2}{175L^2} s' - \frac{4s^2\hbar^3 g}{175ML^4} + \frac{2g\hbar^2}{5L^2} g' - \frac{2g^3\hbar^3}{5ML^4}, \qquad (2.42)
\end{aligned}
$$

where s' and g' are the time derivatives of s and g respectively. Equating the right hand sides of Eqs. (2.41) and (2.42) gives

$$
\begin{aligned}
0 &= \frac{g\hbar^2}{M\omega^2 L_0^3}\left(g' - \frac{g^2\hbar}{ML^2}\right) + \frac{2s\hbar^2}{35M\omega^2 L_0^3}\left(s' - \frac{gs\hbar}{ML^2}\right) \\
&- \frac{g\hbar}{L_0^3}\left(-1+\frac{L_0^3}{2L^3}\right) - \frac{g\hbar}{L} f_2(q) - \frac{2s\hbar}{35L} f_3(q), \qquad (2.43)
\end{aligned}
$$

where $f_2(q)$ function is given by Eq. (2.20) and the function $f_3(q)$ is defined as

$$
f_3(q) = 35q|q|(|q|-1)^2(2|q|^2+4|q|-3)\theta(|q|<1). \qquad (2.44)
$$

The Eq. (2.43) can be rearranged to get,

$$
\begin{aligned}
g' &= \frac{g^2\hbar}{ML^2} + \frac{2s^2\hbar}{35ML^2} - \frac{M\omega^2 L^2}{\hbar}\left(1-\frac{L_0^3}{2L^3}\right) \\
&+ \frac{M\omega^2 L_0^3}{\hbar L} f_2(q) - \frac{2s}{35g}\left(s' - \frac{M\omega^2 L_0^3}{\hbar L} f_3(q)\right). \qquad (2.45)
\end{aligned}
$$

Differentiating the Eq. (2.30) in both sides with respect to t and equating the right hand side of the result to the right hand side of the Eq. (2.37), along with the help of the Eqs. (2.27) and (2.34) gives,

$$g' = \frac{g^2\hbar}{ML^2} + \frac{2s^2\hbar}{35ML^2} - \frac{M\omega^2L^2}{\hbar}\left(1 - \frac{L_0^3}{2L^3}\right) + \frac{M\omega^2L_0^3}{\hbar L}f_2(q). \tag{2.46}$$

where $f_2(q) = -(|q|-1)^2(6|q|^3 + 12|q|^2 - 2|q| - 1)\theta(|q| < 1)$. Then, the Eqs. (2.45) and (2.46) give

$$s' = \frac{M\omega^2L_0^3}{\hbar L}f_3(q). \tag{2.47}$$

From Eqs. (2.34) and (2.47), the equation for v can be obtained as follows:

$$v' = -\omega^2 x_0 + \frac{gs\hbar^2}{10M^2L^3} + \frac{\omega^2L_0^3}{L^2}f_1(q). \tag{2.48}$$

Putting the Eqs. (2.27), (2.32), (2.46), (2.47), and (2.48) together, the equations of motion to various parameters are as follows:

$$\begin{aligned}
L' &= \frac{g\hbar}{ML}, \\
x_0' &= v + \frac{s\hbar}{10ML}, \\
v' &= -\omega^2 x_0 + \frac{gs\hbar^2}{10M^2L^3} + \frac{\omega^2L_0^3}{L^2}f_1(q), \\
g' &= \frac{g^2\hbar}{ML^2} + \frac{2}{35}\frac{s^2\hbar}{ML^2} - \frac{M\omega^2L^2}{\hbar}\left(1 - \frac{L_0^3}{2L^3}\right) + \frac{M\omega^2L_0^3}{\hbar L}f_2(q), \\
s' &= \frac{M\omega^2L_0^3}{\hbar L}f_3(q),
\end{aligned} \tag{2.49}$$

where the f - functions are defined as follows:

$$\begin{aligned}
f_1(q) &= -\frac{q}{2}(|q|-1)^2(14|q|^3 + 28q^2 - 23|q| - 4)\theta(|q| < 1), \\
f_2(q) &= -(|q|-1)^2(6|q|^3 + 12|q|^2 - 2|q| - 1)\theta(|q| < 1), \\
f_3(q) &= 35q|q|(|q|-1)^2(2|q|^2 + 4|q| - 3)\theta(|q| < 1).
\end{aligned} \tag{2.50}$$

The parameter $q = x_0/L$ in Eq. (2.50) is the relative position of the center of mass of a harmonic. The θ-function in Eq. (2.50) is equal to one if its argument is a logical true and zero if it is a logical false. These functions arise because of the interatomic interactions between the two harmonics. Therefore, they are non-zero only when the harmonics are overlapping. In the left hand side of Eq. (2.49), a variable with a prime symbol is a derivative of the variable with respect to time.

2.4.4 Normalized equations

We slightly reorganize the terms in Eq. (2.49) and express them in dimensionless form by using the normalization introduced in Sections 2.2 and 2.3.2 as follows:

$$\begin{aligned} R_\tau &= \frac{G}{R}, \\ G_\tau &= \frac{G^2}{R^2} - R^2\left(1 - \frac{1}{2R^3}\right) + \frac{1}{R}d_2(q), \\ (X_0)_\tau &= V + \frac{S}{10R}, \\ \left(V + \frac{S}{10R}\right)_\tau &= -X_0 + \frac{d_1(q)}{R^2}, \\ S_\tau &= \frac{d_3(q)}{R}, \end{aligned} \tag{2.51}$$

where $(x)_\tau$ represents the derivative of the variable x with respect to time. We define the d-fucntions

$$\begin{aligned} d_1(q) &= q(|q|-1)^2(|q|+2)\theta(|q|<1), \\ d_2(q) &= (|q|-1)^2(-6|q|^3 - 12|q|^2 + 2|q| + 1)\theta(|q|<1), \\ d_3(q) &= 35q|q|(|q|-1)^2(2|q|^2 + 4|q| - 3)\theta(|q|<1), \end{aligned} \tag{2.52}$$

which we use in the analysis of Eq. (2.51). For the analysis of Eq. (2.51), we also need to evaluate the functions $D_i(q) = \int_0^q d_i(x)dx$, which are integrals of the functions

$d_i(q)$, with respect to q and they are as follows:

$$\begin{aligned} D_1(q) &= \frac{1}{5}q^2(|q|^3 - 5|q| + 5), \\ D_2(q) &= -q(|q| - 1)^3(q^2 + 3|q| + 1), \\ D_3(q) &= \frac{1}{2}|q|^3(20q^4 - 126q^2 + 175|q| - 70). \end{aligned} \tag{2.53}$$

Expressions for the functions $D_i(q)$ given by Eq. (2.53) are valid in the region $|q| < 1$. For $|q| \geq 1$, the functions $D_i(q)$ are constant and equal to their boundary values : $D_1(\pm 1) = 1/5$, $D_2(\pm 1) = 0$, and $D_3(\pm 1) = -1/2$.

2.4.5 Smallness parameters and the order of magnitude

In deriving the equations of motion (Eq. 2.51), ϵ and V_0^{-1} were used as smallness parameters and terms of the order of ϵ^2 and V_0^{-2} have been neglected. This can be justified by the following estimate. For a BEC of ^{87}Rb atoms, $v_0 = 11.7$ mm/s . For the longitudinal angular frequency $\omega = 2\pi \times 4.1$ Hz , the angular frequency in the transverse dimensions $\omega_\perp = 2\pi \times 80$ Hz [48], and the number of atoms in the condensate $N = 10^4$ [31], the equilibrium size of a condensate L_0 given by Eq. (2.3) is approximately 40 μm. For these parameters, the inverse of the dimensionless initial speed V_0 of the harmonics is $V_0^{-1} \approx 0.09$ and $\epsilon \approx 0.018$.

2.4.6 Evolution of the radius and the quadratic phase

When the clouds are not overlapping, the terms containing $d_2(q)$ in the second of Eq. (2.51) is zero. Then, we can write the second of Eq. (2.51) as follows:

$$G_\tau = \frac{G^2}{R^2} - R^2\left(1 - \frac{1}{2R^3}\right). \tag{2.54}$$

Differentiating the first of Eq. (2.51) in both sides with respect to τ and then making substitutions of R_τ from the the first of Eq. (2.51) and G_τ from Eq. (2.54) in the

resulting equation,

$$R_{\tau\tau} = -R\left(1 - \frac{1}{2R^3}\right) = -R + \frac{1}{2R^2}, \tag{2.55}$$

where $R_{\tau\tau}$ is the second derivative of R with respect to τ. Multiplying both sides of the Eq. (2.55) by $2dR/d\tau$ and integrating with initial conditions, $R(0) = 1$ and $R_\tau(0) = 0$ results into the following equation:

$$R_\tau^2 \;=\; 2 - \frac{1}{R} - R^2, \tag{2.56}$$

which can be written as

$$R_\tau \;=\; \pm\sqrt{\frac{(1-R)(R^2+R-1)}{R}}. \tag{2.57}$$

Then, from the first of Eq. (2.51), the solution for G,

$$G(\tau) = \pm\sqrt{R(1-R)(R^2+R-1)}. \tag{2.58}$$

The solutions to R and G come to be the elliptic functions. It is important to notice that Eq. (2.57) for R (and hence Eq. (2.58) for G) is "universal", i.e., independent of the trap frequencies, number of atoms in the condensate, etc., and needs to be solved only once. Figure 2.2 shows the time evolution of R and G for a full trap period obtained by solving the first two of Eq. (2.51) numerically. The small kinks in the plot of G during splitting, at recombination, and when the harmonics pass through each other, are due to mutual interaction between the two harmonics at overlap (the term with d_2 in equation for G_τ). Figure 2.2 shows that obtaining Eq. (2.57) for R_τ by neglecting the term containing $d_2(q)$ in the second of Eq. (2.51) is an excellent approximation. It is interesting to note that the period of oscillations of the radius is about 60% of the trap period. The quadratic phase G has the same period of oscillation as that of R.

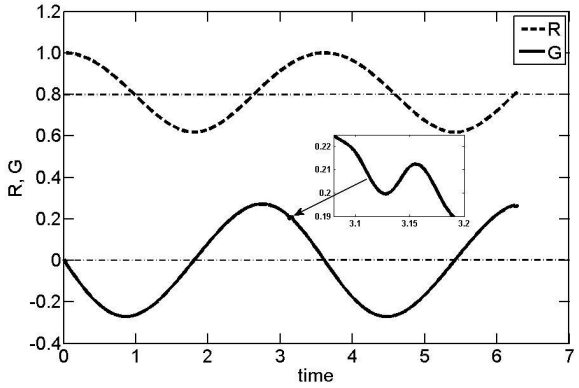

Figure 2.2 Time evolution of the dimensionless radius R of a harmonic and the quadratic phase G (rad) for a trap period. The horizontal axis is dimensionless time from 0 to 2π. The inset shows the effect of interatomic interactions on G when the two harmonics pass through each other.

The numerical values of R and G at times, $\tau = [0,\ \pi/2,\ \pi,\ 3\pi/2,\ 2\pi]$ are as follows: $R = [1,\ 0.64,\ 0.95,\ 0.76,\ 0.81]$ and $G = [0,\ -0.098,\ 0.206,\ -0.247,\ 0.268]$. In our analysis, we shall need the values of R and G at the time of recombination $\tau = 2\pi$: $R(2\pi) \approx 0.81$ and $G(2\pi) \approx 0.27$.

2.4.7 Evolution of the cubic phase

Evolution of the cubic phase $S(q)$ is governed by the last of Eq. (2.51). The cubic phase changes only when the harmonics overlap because, otherwise, the function $d_3(q)$ in (Eq. 2.52) is zero. Integration of the last of Eq. (2.51) yields

$$S(q) = \int_0^\tau d\tau' \frac{d_3(q)}{R} = \int_0^q dq \frac{d_3(q)}{R}\frac{d\tau}{dq} \approx \frac{D_3(q)}{V_0}, \tag{2.59}$$

because in the region of overlap, $dq/d\tau \approx \pm V_0/R$ and $S(0) = 0$. The function $D_3(q)$ is given by the last of Eq. (2.53). After the first separation of the harmonics, the

value of S outside the overlap region is

$$S(1) = -\frac{1}{2V_0}, \tag{2.60}$$

because $D_3(1) = -1/2$. The difference between the values of S before and after the passage of the harmonics through each other around mid-cycle $\tau \approx T/2$ is zero because its calculation involves integration of the odd function $d_3(q)$ from $q = 1$ to $q = -1$. Finally, near the end of the cycle

$$S(q) - S(-1) = \frac{1}{V_0}\left[D_3(q) - D_3(-1)\right]. \tag{2.61}$$

Combining Eqs. (2.60) and (2.61), the value of S near the end of the cycle

$$S(\tau \approx 2\pi) = \frac{D_3(q)}{V_0} \approx -\frac{35|q|^3}{V_0}. \tag{2.62}$$

in the lowest order of $|q|$.

Figure 2.3 shows the evolution of S with time. It is zero initially and grows to a negative peak once the two harmonics start moving away from each other. After the harmonics completely separate, the value of S remains constant at its boundary value. The inset in Figure 2.3 shows the evolution of S when the two harmonics pass through each other.

2.4.8 Energy of the condensate

The energy of the condensate is given by the expectation value of the Hamiltonian with respect to the wave function ψ as it follows:

$$E = \langle\psi|H|\psi\rangle = \int_{-\infty}^{\infty} dx\psi^* \left[-\frac{\hbar^2}{2M}\frac{\partial^2}{\partial x^2} + \frac{1}{2}M\omega^2 x^2 + \frac{g_{1D}}{2}|\psi|^2\right]\psi. \tag{2.63}$$

Substituting $\psi = (1/\sqrt{2})(\psi_+ + \psi_-)$ in Eq. (2.63) gives

$$E = -\frac{\hbar^2}{4M}\int_{-\infty}^{\infty} dx \left(\psi_+^*\frac{\partial^2\psi_+}{\partial x^2} + \psi_+^*\frac{\partial^2\psi_-}{\partial x^2} + \psi_-^*\frac{\partial^2\psi_+}{\partial x^2} + \psi_-^*\frac{\partial^2\psi_-}{\partial x^2}\right)$$

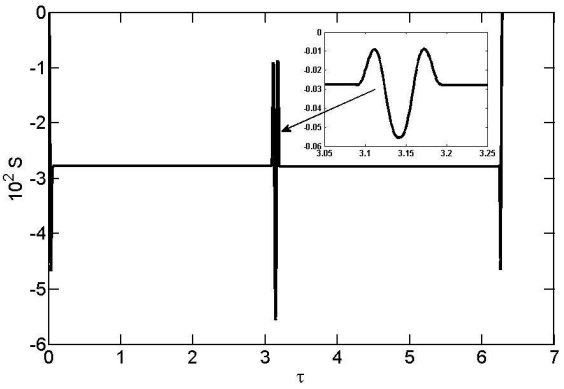

Figure 2.3 Time evolution of the cubic phase S(rad). The horizontal axis is dimensionless time, τ from 0 to 2π. The cubic phase develops only when the clouds overlap during splitting, when they pass through each other and when they recombine. The inset shows the evolution of S when the clouds pass through each other.

$$
\begin{aligned}
&+ \quad \frac{1}{4}M\omega^2 \int_{-\infty}^{\infty} dx \left(x^2|\psi_+|^2 + x^2|\psi_-|^2 + x^2\psi_+^*\psi_- + x^2\psi_-^*\psi_+ \right) \\
&+ \quad \frac{g_{1D}}{8} \int_{-\infty}^{\infty} dx \left(|\psi_+|^4 + |\psi_-|^4 + 2|\psi_+|^2\psi_+\psi_-^* + 2|\psi_-|^2\psi_+^*\psi_- + (\psi_+^*)^2(\psi_-)^2 + (\psi_+)^2(\psi_-^*)^2 \right) \\
&+ \quad \frac{g_{1D}}{4} \int_{-\infty}^{\infty} dx \left(|\psi_+|^2\psi_+^*\psi_- + |\psi_-|^2\psi_+\psi_-^* + 2|\psi_+|^2|\psi_-|^2 \right). \qquad (2.64)
\end{aligned}
$$

which can be simplified to

$$
\begin{aligned}
E \quad &= \quad -\frac{\hbar^2}{4M} \int_{-\infty}^{\infty} dx \left(\psi_+^* \frac{\partial^2\psi_+}{\partial x^2} + \psi_+^* \frac{\partial^2\psi_-}{\partial x^2} + \psi_-^* \frac{\partial^2\psi_+}{\partial x^2} + \psi_-^* \frac{\partial^2\psi_-}{\partial x^2} \right) \\
&+ \quad \frac{1}{4}M\omega^2 \int_{-\infty}^{\infty} dx \left(n_+x^2 + n_-x^2 + x^2\psi_+^*\psi_- + x^2\psi_-^*\psi_+ \right) \\
&+ \quad \frac{g_{1D}}{8} \int_{-\infty}^{\infty} dx \left[n_+^2 + n_-^2 + 4n_+n_- + 2(n_+ + n_-)(\psi_+^*\psi_- + \psi_+\psi_-^*) + (\psi_+^*)^2(\psi_-)^2 + (\psi_-^*)^2(\psi_+)^2 \right]. \qquad (2.65)
\end{aligned}
$$

For the $\psi_\pm = \sqrt{n_\pm}\exp(i\phi_\pm)$, the order of the term $\epsilon = \int dx\psi_+\psi_- \approx 1/(kL)$. Integration by parts reduces the expression for energy (Eq. 2.65) to the following form:

$$
E \quad = \quad \frac{1}{2}\int dx \left[\frac{\hbar^2}{2M} \left(\left| \frac{\partial\psi_+}{\partial x} \right|^2 + \left| \frac{\partial\psi_-}{\partial x} \right|^2 \right) + V(x)\,(n_+ + n_-) \right.
$$

$$+ \quad \frac{g_{1D}}{4}\left(n_+^2 + n_-^2 + 4n_+n_-\right)\Big], \tag{2.66}$$

where we have neglected the terms of the order of ϵ and its higher powers. The potential $V(x) = \frac{1}{2}M\omega^2x^2$. After some algebra, and $g_{1D} = (2/3)M\omega^2L_0^3$, the final expression for the energy of the system (split-clouds in a harmonic trap) is:

$$\begin{aligned} E &= \frac{M}{2}\left(v + \frac{s\hbar}{10ML}\right)^2 + \frac{g^2\hbar^2}{10ML^2} + \frac{1}{175}\frac{s^2\hbar^2}{ML^2} \\ &+ \frac{1}{2}M\omega^2\left(x_0^2 + \frac{L^2}{5}\right) + \frac{M\omega^2L_0^3}{10L}\left[1 - 2(|q|-1)^3(q^2+3|q|+1)\theta(|q|<1)\right] \\ &= E_K + E_P + E_N, \end{aligned} \tag{2.67}$$

where

$$\begin{aligned} E_K &= \frac{M}{2}\left(v + \frac{s\hbar}{10ML}\right)^2 + \frac{g^2\hbar^2}{10ML^2} + \frac{1}{175}\frac{s^2\hbar^2}{ML^2}, \\ E_P &= \frac{1}{2}M\omega^2\left(x_0^2 + \frac{L^2}{5}\right), \\ E_N &= \frac{M\omega^2L_0^3}{10L}\left[1 - 2(|q|-1)^3(q^2+3|q|+1)\theta(|q|<1)\right]. \end{aligned} \tag{2.68}$$

In Eq. (2.68), E_K is the total kinetic energy of the system. It depends upon the velocity of the clouds, the quadratic and the cubic phases. The kinetic energy right after splitting is proportional to V_0^2 but, when the clouds evolve with time, the quadratic and the cubic phases develop and the kinetic energy has terms containing speed as well as these phases. The term E_P is potential energy of the clouds. This energy is equal to the sum of the potential energy of the condensate in the trap caused by its finite size, and the potential energy due to the displacement of the center of mass of each cloud after splitting. Due to its finite size, a cloud has non-zero potential energy even when it is at the bottom of the trap. The term E_N is nonlinear energy due to atom-atom interactions in the condensate. During the interferometric time between the splitting and recombination pulse, the total energy of the system is conserved.

2.5 Recombination

2.5.1 The wave function at recombination

The split clouds are recombined when they overlap at the end of the interferometric cycle by the application of a recombination pulse. A recombination pulse consists of a sequence of two subpulses as that in a splitting pulse. The whole idea of recombination is to compensate the effect of splitting on the BEC clouds. The clouds would come to rest completely if there is no phase accumulated in between, but this does not happen so, because of the accumulation of a phase due to environment and the atom-atom interactions in the condensate. Therefore, the wave function of the zero momentum cloud right after the recombination pulse is applied,

$$\psi_0(x,x_0) = \frac{1}{2}\left[\sqrt{n_+(x-x_0)}e^{i(\phi_+ - \frac{Mv_0}{\hbar}x)} + \sqrt{n_-(x+x_0)}e^{i(\phi_- + \frac{Mv_0}{\hbar}x)}\right], \qquad (2.69)$$

where $2\hbar k = Mv_0$ has been used. The factor of $1/2$ in the RHS of above equation appears because of the splitting matrix [45] which is applied twice, during splitting and during recombination. Each time, a factor of $1/\sqrt{2}$ enters giving rise to a factor of $1/2$. Using the expression for $\phi_\pm$ (Eq. 2.7), the wave function at recombination becomes:

$$\begin{aligned}\psi_0(x,x_0) &= \frac{1}{2}\left[\sqrt{n_+(x-x_0)}e^{i\left(\phi_{0,+} + \frac{M}{\hbar}(v-v_0)x + \frac{g}{2L^2}(x-x_0)^2 + \frac{s}{6L^3}(x-x_0)^3 - \frac{Mv}{\hbar}x_0\right)}\right. \\ &+ \left.\sqrt{n_-(x+x_0)}e^{i\left(\phi_{0,-} - \frac{M}{\hbar}(v-v_0)x + \frac{g}{2L^2}(x+x_0)^2 - \frac{s}{6L^3}(x+x_0)^3 - \frac{Mv}{\hbar}x_0\right)}\right]. \qquad (2.70)\end{aligned}$$

Since we are interested only in the spatially-dependent relative phase, we drop the overall phase factor, $\exp\left(-i\frac{Mv}{\hbar}x_0\right)$ and also neglect the only time dependent phase factors, $\exp(i\phi_{0,+})$ and $\exp(i\phi_{0,-})$. Then we can write the wave function at recombination as

$$\psi_0(x,x_0) \approx \frac{1}{2}\left[\sqrt{n_+(x-x_0)}e^{i\left(+\frac{M}{\hbar}(v-v_0)x + \frac{g}{2L^2}(x-x_0)^2 + \frac{s}{6L^3}(x-x_0)^3\right)}\right.$$

$$+ \quad \sqrt{n_-(x+x_0)}e^{i\left(-\frac{M}{\hbar}(v-v_0)x+\frac{g}{2L^2}(x+x_0)^2-\frac{s}{6L^3}(x+x_0)^3\right)}\Big]. \qquad (2.71)$$

In the dimensionless variables, the wave function at recombination becomes

$$\begin{aligned}\psi_0(X,X_0) &\approx \frac{1}{2}\Big[\sqrt{n_+(X-X_0)}e^{\frac{i}{\epsilon}\left(+(V-V_0)X+\frac{G}{2R^2}(X-X_0)^2+\frac{S}{6R^3}(X-X_0)^3\right)} \\ &+ \sqrt{n_-(X+X_0)}e^{\frac{i}{\epsilon}\left(-(V-V_0)X+\frac{G}{2R^2}(X+X_0)^2-\frac{S}{6R^3}(X+X_0)^3\right)}\Big]. \qquad (2.72)\end{aligned}$$

After some algebra, Eq. (2.72) gives,

$$\psi_0(\xi,q) \approx \frac{1}{2}\left[\sqrt{n_+(\xi-q)}e^{i(\Delta K\xi+\Gamma\xi^3)}+\sqrt{n_-(\xi+q)}e^{-i(\Delta K\xi+\Gamma\xi^3)}\right], \qquad (2.73)$$

where

$$\begin{aligned}\Delta K &= \frac{R}{\epsilon}\left(V-V_0-\frac{GX_0}{R^2}+\frac{SX_0^2}{2R^3}\right), \\ \Gamma &= \frac{S}{6\epsilon}, \qquad (2.74)\end{aligned}$$

and $\xi = X/R$ is the normalized coordinate and $q = X_0/R$ is the normalized position of the center of mass. In getting the above equation for $\psi_0(\xi,q)$, the terms which will be canceled in obtaining the relative phase have been discarded. These terms are $(G/2R^2 - SX_0/2R^3)X^2$ and $(GX_0^2/2R^2 - SX_0^3/6R^3)$ in the phase associated with the wave functions ψ_+ and ψ_- each. Since they have same signs, they will cancel when we compute the relative phase between the two clouds.

2.5.2 Probability density at recombination

Assuming that the density enevelopes of two zero momentum harmonics perfectly overlap each other at recombination, we can write, $\sqrt{n_+(\xi-q)} = \sqrt{n(\xi)} = \sqrt{n_-(\xi+q)}$. This simplifies Eq. (2.73) for the wave function of the zero momentum harmonic to

$$\begin{aligned}\psi_0(\xi,q) &\approx \sqrt{n(\xi)}\left[\frac{1}{2}\left(e^{i(\Delta K\xi+\Gamma\xi^3)}+e^{-i(\Delta K\xi+\Gamma\xi^3)}\right)\right] \\ &= \sqrt{n(\xi)}\cos(\Delta K\xi+\Gamma\xi^3). \qquad (2.75)\end{aligned}$$

The probability density for atoms to be in the zero momentum state at recombination

$$|\psi_0(\xi,q)|^2 \approx n(\xi)\cos^2(\Delta K\xi+\Gamma\xi^3). \tag{2.76}$$

The argument of the cosine function in Eq. (2.76) is the total spatial phase across the split clouds, i.e.,

$$\Phi(\xi)=\Delta K\xi+\Gamma\xi^3, \tag{2.77}$$

where ΔK and Γ are given by Eq. (2.74). The spatial phase therefore affects the population distribution in the zero momentum clouds at recombination.

2.5.3 Relative population at recombination

The relative population in the central cloud after the recombination is given by

$$\begin{aligned}\frac{N_0}{N_{tot}} &= \int|\psi_0|^2d\xi=\frac{1}{2}+\frac{3}{4}\int_0^{1-|q|}d\xi[(1-\xi^2-q^2)^2-4\xi^2q^2]^2\cos(\Delta K+\Gamma\xi^3)\\ &= \frac{1}{2}+\frac{3}{4}\int_{|q|}^1 dx(x^2-q^2)^{1/2}[(2-x)^2-q^2]^{1/2}\cos\left[\Delta K(1-x)+\Gamma(1-x)^3\right],\end{aligned} \tag{2.78}$$

where $|\psi_0|^2$ is given by Eq. (2.76) and N_{tot} is the total number of atoms. Using the fact that

$$\begin{aligned}\int_{|q|}^1 dx(x^2-q^2)^{1/2}[(2-x)^2-q^2]^{1/2} &\approx -\frac{q^2}{2}(2\ln 2-1)+\int_{|q|}^1 dx(2-x)\sqrt{x^2-q^2}\\ &= \frac{2}{3}+q^2\left(\ln|q|-2\ln 2+\frac{1}{2}\right),\end{aligned}$$

the relative population of the atoms in the central cloud at recombination,

$$\frac{N_0}{N_{tot}}=1+\frac{3q^2}{4}\left(\ln|q|-2\ln 2+\frac{1}{2}\right)-\frac{1}{5}\left[(\Delta K)^2+\frac{6}{7}\Delta K\Gamma+\frac{5}{21}\Gamma^2\right]. \tag{2.79}$$

2.5.4 Contrast of interferometric fringes

The contrast of interferometric fringes V, defined by $V = 2(N_0/N_{tot}) - 1$ [45] will be given by the following expression:

$$V \approx 1 - \frac{2}{5}\left[(\Delta K)^2 + \frac{6}{7}\Delta K\Gamma + \frac{5}{21}\Gamma^2\right], \tag{2.80}$$

where we have used Eq. (2.79) and assumed that the density envelopes completely overlap ($q = 0$) at recombination.

2.5.5 Velocity and total spatial phase at recombination

The velocity of the split clouds at recombination can be obtained from the conservation principle. The total energy of the system of the split clouds (Eq. 2.67) in the trap

$$\begin{aligned} E_T &= \frac{1}{2}\left(V + \frac{S}{10R}\right)^2 + \frac{G^2}{10R^2} + \frac{S^2}{175R^2} \\ &+ \frac{1}{2}\left(X_0^2 + \frac{R^2}{5}\right) + \frac{1}{10R}\left[1 + 10qd_1 + 2d_2\right], \end{aligned} \tag{2.81}$$

in the dimensionless variables. The $d_1(q)$ and $d_2(q)$ functions in Eq. (2.81) are the overlap functions and given by Eq. (2.52). The total energy (E_T) has been normalized to a factor of $M\omega^2 L_0^2$. In Eq. (2.81), S and G are the cubic and quadratic phases respectively. Both of these phases are zero at $\tau = 0$ (see Figure 2.2 and Figure 2.3). At this time, since the clouds are on top of each other, $X_0 = 0$, $d_1(q) = 0$, $d_2(q) = 1$, and $R = L/L_0 = L_0/L_0 = 1$, where L_0 is the equilibrium size (half-radius) of each cloud. Therefore, the total energy of the system at this time, (i.e, at $\tau = 0$),

$$E_T(\tau = 0) = \frac{1}{2}V_0^2 + \frac{1}{10}R_0^2 + \frac{3}{10R_0}, \tag{2.82}$$

where V_0 is the dimensionless initial speed of each cloud.

To find the energy at subsequent times, especially at $\tau = T$, the recombination time, we do the following estimates. Since $S' = d_3(q)/R$, $S(q) = \int_0^\tau d_3(q)/R d\tau'$, where $d_3(q) = 35q|q|(|q|-1)^2(2q^2+4|q|-3)\theta(|q|<1)$. Consider the time at which clouds separate at first (beam splitting operation), $R \approx R_0$ (radius does not change by much during this time). Also $X_0 = V_0\tau'$ gives $dX_0 = V_0 d\tau'$. But $q = X_0/R$ and therefore, $dq = (V_0/R_0)d\tau'$. Making all these substitutions gives $S(q) = D_3(q)/V_0$, where $D_3(q) = (1/2)|q|^3(20q^4 - 126q^2 + 175|q| - 70)$. At $q = 1$, $D_3(q) = -1/2$. Therefore, $S(q=1) = -1/(2V_0)$ when the two clouds just separate, and it remains constant at this value. Therefore, the cubic phase $S(q) \sim 1/V_0$. From the numerical solutions of the equations for R and G, we can see that $R \sim 1$ and $G \sim 1$ in our dimensionless variable, no matter what the trap frequency and the initial size of the clouds are. At recombination, $q << 1$ because $X_0 << R_T$ at this time. Since $V \sim V_0$ at $\tau = T$, and $S \propto 1/V$ gives $VS \sim 1$. Since $q << 1$, we are going to retain the terms only of the order of q, and the constant terms. We neglect the term $(10qd_1(q))$, which has q^2 as the lowest order term, but we retain $(2d_2(q))$ because the lowest order term in this is 2, which is a constant. Also $X_0^2 = q^2R_T^2$, which is of the order of q^2 is neglected. Therefore, the total energy of the system at $\tau = T$ can be approximated as:

$$E_T = \frac{1}{2}V^2 + \frac{G_T^2}{10R_T^2} + \frac{R_T^2}{10} + \frac{3}{10R_T}. \tag{2.83}$$

The energy conservation principle (from Eq. (2.82) and Eq. (2.83)) then gives the speed of each cloud at recombination as follows:

$$V(\tau = T) \approx V_0\left[1 + \frac{1}{2V_0^2}\left(\frac{4}{5} - \frac{G_T^2}{5R_T^2} - \frac{R_T^2}{5} - \frac{3}{5R_T}\right)\right], \tag{2.84}$$

which gives the difference between the velocity at recombination and the initial velocity as

$$V - V_0 \approx -\frac{1}{2V_0}\left(\frac{G_T^2}{5R_T^2} + \frac{R_T^2}{5} + \frac{3}{5R_T} - \frac{4}{5}\right). \tag{2.85}$$

The expression for ΔK at time $\tau = T$ (Eq. 2.74),

$$\Delta K = \frac{R_T}{\epsilon}\left(V - V_0 - \frac{G_T X_0}{R_T^2} + \frac{S X_0^2}{2R_T^3}\right). \tag{2.86}$$

Substituting $R_0 = 1$, $R_T = 0.81R_0 = 0.81$, $X_0/R_T = q$, $V \approx V_0$, and $G_T \approx 0.27$, and using the expression for $(V - V_0)$ from the Eq. (2.85) into the Eq. (2.86),

$$\Delta K = -\frac{1}{\epsilon}\left(\frac{0.04}{V_0} + 0.27q\right). \tag{2.87}$$

From the second of Eq. (2.74) and Eq. (2.62), the expression for the cubic phase,

$$\Gamma = -\frac{35}{6\epsilon V_0}|q|^3. \tag{2.88}$$

Therefore, the coordinate dependent phase between the two clouds (Eq. 2.77) at recombination,

$$\Phi(\xi) = -\frac{1}{\epsilon}\left[\left(\frac{0.04}{V_0} + 0.27q\right)\xi + \frac{35}{6V_0}|q|^3\xi^3\right]. \tag{2.89}$$

2.5.6 Theoretical limits of performance

The best theoretical limits of performance of the interferometer can be obtained by maximizing the contrast given by Eq. (2.80). For this we need to minimize the bracketed term in the right hand side of Eq. (2.80). To simplify the calculation, we write ΔK (Eq. 2.87) and Γ (Eq. 2.88) as $\Delta K = -(a + bq)$, $\Gamma = -c|q|^3$, where $a = 0.04/\epsilon V_0$, $b = 0.27/\epsilon$ and $c = 35/(6\epsilon V_0)$. For $q \geq 0$, the phase (Eq. 2.89) starts with negative linear slope ΔK and then gets more negative for larger values of ξ. For large enough negative values of q such that $\Delta K \geq 0$ the phase starts with positive linear slope and then flattens out somewhat. It is clear that the optimum value of q that minimizes the phase corresponds to negative values of q such that ΔK is small and positive. In this case, the phase starts with positive slope but then becomes negative as ξ increases. To get a quantitative estimate, the bracketed term in the

right hand side of Eq. (2.80) is minimized. Assuming that this minimization happens close to $q = -a/b$, we can write $q = -(a/b)(1+\delta)$ and represent the last term in Eq. (2.80) as

$$0 = -\frac{2}{5}\left[a^2\delta^2 - \frac{6}{7}a\delta c\left(\frac{a}{b}\right)^3 + \frac{5}{21}c^2\left(\frac{a}{b}\right)^6\right], \tag{2.90}$$

with the minimum at

$$\delta = \frac{3}{7}\frac{c}{a}\left(\frac{a}{b}\right)^3 = \frac{0.20}{V_0^3} \ll 1. \tag{2.91}$$

For this value of δ (and hence q), $\Delta K = 8\times10^{-3}/\epsilon V_0^4$, $\Gamma = -0.023/\epsilon V_0^4$. Therefore, from Eq. (2.89), the relative phase between the two clouds,

$$\Phi(\xi) = \frac{0.008}{\epsilon V_0^4}\xi - \frac{0.023}{\epsilon V_0^4}\xi^3. \tag{2.92}$$

Requiring a small phase change $|\Phi| \leq 1$ (see Section 2.5.9), we obtain an inequality

$$\frac{0.01}{\epsilon V_0^4} \leq 1, \tag{2.93}$$

for a high contrast of the interferometer fringes. The inequality (2.93) in terms of dimensional variables reads

$$\left(\frac{\hbar\omega_\perp^2\omega a_s^2}{10Mv_0^4}\right)^{1/2} N \leq 1. \tag{2.94}$$

The inequality (Eq. 2.94) gives the fundamental theoretical limit of performance of a guided wave BEC-based free oscillation interferometer in terms of the experimental parameters: the trap frequencies, the number of atoms in the condensate, and the velocity imparted to the clouds by the splitting laser pulses. Eq. (2.94) shows that for a tighter trap, we need to use a smaller number of atoms so that the interferometer gives better contrast with reduced nonlinearity. For a weaker trap, the number of atoms in the condesnate can be more. There can be other technical limitations like noise (caused by vibrations), misalignment of the splitting laser pulse, etc., which will prevent from achieving the fundamental limit of the interferometer.

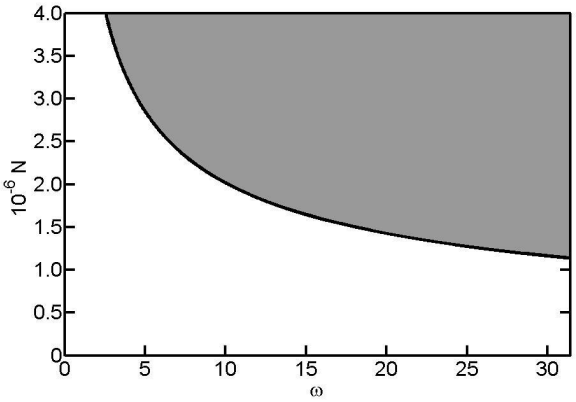

Figure 2.4 Working region in parameter space of a free oscillation interferometer, with the longitudinal trap frequency ω (rad/s) and the total number of atoms N in the condensate. The interferometer works in the unshaded region and does not work in the shaded region.

The working region of the interferometer in parameter space for the transverse trapping frequency $\omega_\perp = 2\pi \times 80$Hz is shown in Figure 2.4. In the region below the boundary line (which has been obtained taking the equality sign in Eq. (2.94)), the interferometric contrast exceeds 50 %. The maximum number of atoms corresponding to the boundary region for a given trap can be read directly from the graph. For example, for $\omega = 2\pi \times 4.1$Hz , $N \approx 10^6$ and the interferometric cycle time is 244 milliseconds (the trap period).

2.5.7 Optimized interferometric contrast

The spatial phase given by Eq. (2.92) is a maximum on the edge of a split cloud where $\xi = 1$. This means that this is the maximum spatial phase when the bracketed term in the expression for the contrast (Eq. 2.80) is a minimum. Then from Eqs. (2.94)

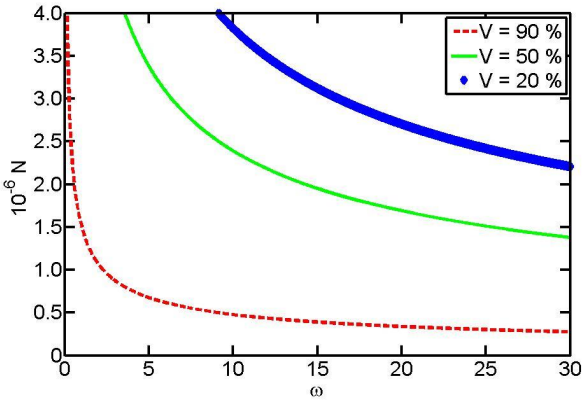

Figure 2.5 The number of atoms N in a condensate as a function of longitudinal frequency ω (rad/s) at various values of the interferometric contrast.

and (2.80), the maximum value of the contrast,

$$V \approx 1 - \frac{2}{5}\left(\frac{\hbar\omega_\perp^2 \omega a_s^2}{10 M v_0^4}\right)^{1/2} N, \tag{2.95}$$

in the dimensional experimental parameters. The number of atoms in a condensate as a function of trap frequencies and the contrast is then given by

$$N \approx \frac{5}{2}(1-V)\left(\frac{10 M v_0^4}{\hbar\omega_\perp^2 a_s^2}\right)^{1/2} \frac{1}{\sqrt{\omega}}. \tag{2.96}$$

Figure 2.5 shows plots of the number of atoms N in the condensate as a function of the longitudinal trap frequency, ω for three different values of contrast. The transverse trapping frequency in these plots, $\omega_\perp = 2\pi \times 80$ Hz. We can find the number of atoms for a given contrast directly from the figure as in Figure 2.4.

2.5.8 Incompletely overlapped situation

If the two clouds do not completely overlap at the time of recombination, the analysis of the interferometer becomes more complicated. This will further increase the loss

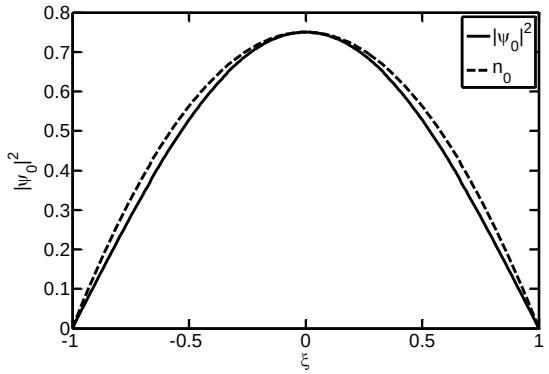

Figure 2.6 The probability density $|\psi_0|^2$ as a function of the coordinate ξ for $\Delta K = 0.5$ and $\Gamma = 0$. The probability density varies smoothly under the density envelope at small ΔK.

of contrast. The effect of incomplete overlap on the interferometric contrast has been investigated in detail in [46, 47].

2.5.9 Effects of large ΔK and Γ

The wave function of the zero momentum harmonic just after the recombination is given by the Eq. (2.75) and the coordinate dependent phase accumulated by the zero momentum harmonic is given by Eq.(2.77). The second term in this phase is much smaller than the first term. Therefore, for $\Delta K\xi$ is much smaller than 1, the phase profile smoothly overlaps on top of the density envelope as shown in Figure 2.6.

Once the first term in phase grows towards 1, a distortion appears on the phase profile. For $\Delta K\xi > 1$, the phase profile oscillates several times under the density envelope as shown in Figure 2.7. The ratio N_0/N_{tot} becomes 1/2 for a large $\Delta K\xi$. Since the contrast of the interference fringes is given by $V = 2(N_0/N_{tot}) - 1$ [45], the contrast goes to zero for $\Delta K\xi > 1$. Therefore, a large ΔK and hence a large spatial

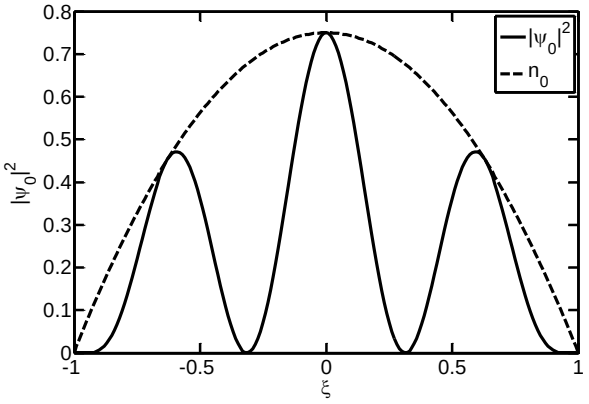

Figure 2.7 The probability density $|\psi_0|^2$ as a function of the coordinate ξ for $\Delta K = 5$ and $\Gamma = 0$. The probability density oscillates several times under its envelope that reduces the contrast of the interference fringes.

relative phase between the clouds at recombination wipes the interference fringes. This justifies why we have taken $|\Phi(\xi)| \leq 1$ to obtain the best working region for an interferometer in the parametric space (Eq. 2.94).

2.6 Conclusions

In this chapter, we analyzed the operation of a BEC-based free oscillation interferometer with optical splitting and recombination of the BEC clouds. Our one-dimensional (1D) analytical model is based on the mean field approximation in the Thomas-fermi limit. From the 1D Gross-Pitaevskii equation, we derived a closed set of ordinary differential equations for the parameters describing the shape of the density envelope and the spatially-varying phase of the BEC clouds. The derivation is based on the equations of motion for the quantum-mechanical expectation values associated with these parameters. The main result of this chapter is Eq. (2.94), which gives the working region of the interferometer in the parameter space and shows how the per-

formance of the interferometer depends on various parameters of the experiment such as the number of particles, longitudinal and transverse frequencies of the trap, and the velocity imparted by the splitting laser pulses. Our analysis shows that the reason for the loss of the coherence in a free oscillation interferometer is the oscillations of the density envelopes of the clouds with a period different from the longitudinal period of the trap.

The analysis does not include effects beyond the mean field approximation such as finite-temperature phase fluctuations along the length of the elongated BEC clouds and phase diffusion. Ref. [46] discussed the importance of the phase fluctuations and concluded that they are negligible for the parameters of the recent experiments [31,40,42,48]. The phase diffusion, specifically in the context of atom interferometers with the optical splitting and recombination of the clouds, has been recently analyzed in [51]. Results of this analysis, applied to the case of a free oscillation interferometer, predict that the region of good performance is given by the inequality

$$\left(\frac{a_s}{\bar{a}}\right)^{2/5}\left(\frac{2\pi\bar{\omega}}{\omega}\right)N^{-1/10}\leq 1, \tag{2.97}$$

where $\bar{\omega}=(\omega_\perp^2\omega)^{1/3}$ and $\bar{a}=\sqrt{\hbar/(M\bar{\omega})}$. The model of Ref. [51] goes beyond the mean field approximation by accounting for the mode-entangled nature of the two BEC clouds after the splitting, but does not account for the development of spatially-varying phases caused by atom-atom interaction during the propagation. Thus, the physics behind Eqs. (2.94) and (2.97) is complementary, and both these inequalities have to be evaluated and their values compared for any particular experiment.

The relative importance of the effects due to spatially-varying phases caused by atom-atom interactions and the phase diffusion is given by the left-hand sides of Eqs. (2.94) and (2.97), respectively. The left-hand-side of Eq. (2.94) for the parameters of the experiments by Burke et al. [40] and Horikoshi et al. [41] is much less than

one, and equals about 0.8 in the experiments by Segal et al. [48]. The left-hand-side of Eq. (2.97) for Ref. [40] is small as compared to one and equals to about 0.65 and 1.0 for Refs. [41] and [48], respectively. This shows that the phase diffusion could be partially responsible for the degradation of coherence in [41] and that both the effects discussed in this analysis and the phase diffusion could be at least partially responsible for the loss of contrast in the experiments [48]. The authors of Refs. [40, 41, 48] also list vibrations as a cause for the degradation of the coherence.

In the experiments discussed in this analysis, the frequency of the trap along the guiding direction is much less than those along the transverse directions. The BEC clouds are cigar-shaped with the largest dimension along the weak guiding direction of the trap and are moving along the same direction. This is the reason why a 1D theory is a good approximation to the experimental situation. A possible slight misalignment of the optical splitting pulses can result in a more complicated 2D or 3D motion of the BEC clouds and their rotations. Analysis of such dynamics requires generalization of the 1D model to higher dimensions.

Chapter 3

Single and double reflection atom interferometers

'It's not that I'm so smart, it's just that I stay with problems longer.' - Albert Einstein

3.1 Introduction

In this chapter, we investigate the operation of single and double reflection atom Michelson interferometers in a weak longitudinal and stronger transverse confinements. Unlike in a free oscillation atom interferometers, the atomic wave packets are reflected by laser pulses in these interferometers. The dynamics of the BEC clouds in such interferometers is schematically shown in Figures 3.1 and 3.2. In the figures, the vertical wavy lines represent the laser pulses and the solid inclined lines going from left to right represent the trajectories of the BEC clouds.

A single reflection interferometer shown schematically in Figure 3.1 was proposed and implemented in [31]. An interferometric cycle of time T starts with the splitting of a stationary BEC cloud ψ_0 at the center of the trap. The splitting laser pulses have

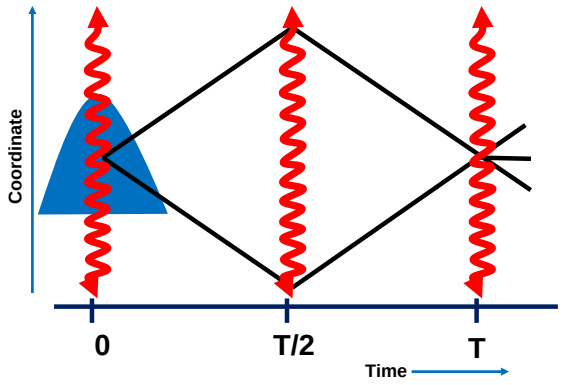

Figure 3.1 A schematic of a single reflection interferometer

the wave vectors $\pm\vec{k}$ and are aligned along the longitudinal dimension of the trap. They act as a diffraction grating for the BEC cloud ψ_0 splitting it into two harmonics ψ_+ (the one moving to the right) and ψ_- (the one moving to the left) [45]. The atoms in the ψ_+ harmonic have velocity, $\vec{v}_0 = +2\hbar\vec{k}/M$ and the atoms in the ψ_- harmonic have velocity, $\vec{v}_0 = -2\hbar\vec{k}/M$ along the axis of the guide. Here M is the atomic mass of the condensate atoms. The two harmonics ψ_+ and ψ_- are then reflected at time $T/2$ by using a laser pulse. A recombination pulse is applied at time T ro recombine the split clouds.

Loss of contrast in a single reflection interferometer is primarily due to the coordinate-dependent phase acquired by the split clouds during the cycle. This phase is caused by the confining potential and the velocity mismatch due to reflection pulses. To overcome this drawback, a double pass interferometer with reflection pulses shown schematically in Figure 3.2 was proposed and implemented in [42]. An interferometric cycle of time T starts with the splitting of the condensate, followed by the reflection of the split clouds at times $T/4$ and $3T/4$ respectively. The split clouds are recombined at time T.

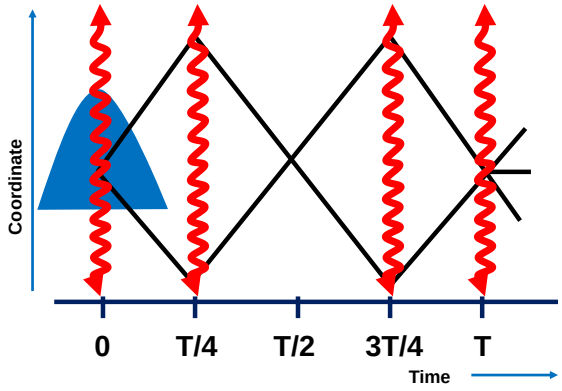

Figure 3.2 A schematic of a double reflection interferometer

In a double reflection interferometer, each cloud travels in both arms of the interferometer before they are finally recombined. Because of the symmetry in the paths followed by the two clouds, the coordinate dependent phase is partially canceled [40]. But the reflection pulses still introduce a velocity mismatch that limits the performance of the interferometer [45].

Several recent experiments have shown that a double reflection interferometer offers an improved contrast compared to a single reflection interferometer. For example, Deissler et al. [37] measure the dynamic polarizability of ^{87}Rb atoms with a double refelction interferometer. Burke et al. [52] show that a double reflection interferometer can be used as a Sagnac interferometer to measure rotation using the Sagnac effect.

A detailed analysis of these interferometer geometries have been performed in [45–47] by expanding the phases in Legendre polynomials and shown that the velocity mismatch introduced by the reflection pulses is the main cause of the loss of contrast in single and double reflection interferometers. In this chapter, we derive the expressions for the differences in velocities at recombination and the splitting in these

interferometers from the equations of motion obtained by evaluating the expectation values of the dynamical quantities and the energy conseravtion principle developed in Chapter 2. These results agree with the results obtained in [45–47], and explain why these geometries have smaller working region in parameter space than that of a free oscillation interferometer.

3.2 Analytic model

The evolution of a split condensate in a weakly-confining parabolic potential of longitudinal frequency ω is described in the framework of the mean-field approximation by Gross-Pitaevskii equation (GPE) which we have explained detail in Chapter 2.

3.2.1 Equations of motion

We derived the equations of motion for various parameters of the split condensates in Section 2.4.3 by evaluating the expectation values of the dynamical quantities describing the split condensate. For convenience, we are giving those equations here again:

$$\begin{aligned} R_\tau &= \frac{G}{R}, \\ G_\tau &= \frac{G^2}{R^2} - R^2\left(1 - \frac{1}{2R^3}\right) + \frac{1}{R}d_2(q), \\ (X_0)_\tau &= V + \frac{S}{10R}, \\ \left(V + \frac{S}{10R}\right)_\tau &= -X_0 + \frac{d_1(q)}{R^2}, \\ S_\tau &= \frac{d_3(q)}{R}, \end{aligned} \tag{3.1}$$

where $(x)_\tau$ represents the derivative of the variable x with respect to time. The d-functions in Eq. (3.1) are as follows:

$$\begin{aligned} d_1(q) &= q(|q|-1)^2(|q|+2)\theta(|q|<1), \\ d_2(q) &= (|q|-1)^2(-6|q|^3-12|q|^2+2|q|+1)\theta(|q|<1), \\ d_3(q) &= 35q|q|(|q|-1)^2(2|q|^2+4|q|-3)\theta(|q|<1). \end{aligned} \tag{3.2}$$

The parameter $q = X_0/R$ in Eq. (3.2) is the relative position of the center of mass of a harmonic. The θ-function in Eq. (3.2) is equal to one if its argument is a logical true and zero if it is a logical false. These functions arise because of the interatomic interactions between the two harmonics. Therefore, they are non-zero only when the harmonics are overlapping.

We also need to evaluate the functions $D_i(q) = \int_0^q d_i(x)dx$, which are integrals of the functions $d_i(q)$, with respect to q and they are as follows:

$$\begin{aligned} D_1(q) &= \frac{1}{5}q^2(|q|^3-5|q|+5), \\ D_2(q) &= -q(|q|-1)^3(q^2+3|q|+1), \\ D_3(q) &= \frac{1}{2}|q|^3(20q^4-126q^2+175|q|-70). \end{aligned} \tag{3.3}$$

Expressions for the functions $D_i(q)$ given by Eq. (3.3) are valid in the region $|q| < 1$. For $|q| \geq 1$, the functions $D_i(q)$ are constant and equal to their boundary values: $D_1(\pm 1) = 1/5$, $D_2(\pm 1) = 0$, and $D_3(\pm 1) = -1/2$.

3.3 Analysis of a single reflection interferometer

In this section, we are deriving an expression for the difference in the velocity of a cloud at recombination and the initial velocity by energy conservation principle.

3.3.1 R and G at small times

In a single reflection interferometer, the reflection pulses are applied a short time after the splitting of the condensate. Therefore, we need to find the expressions for R and G for small times. We can set $R = R_0 = 1$ in solving the first two of Eq. (3.1). Neglecting the terms containing G^2 (which vary as V_0^{-2}), the equation for G_τ can be approximated to

$$G_\tau \approx -\frac{1}{2} + d_2(q), \tag{3.4}$$

where $d_2(q)$ is given by the second of Eq. (3.2). The solution for G before the reflection pulse is applied:

$$G(\tau) = -\frac{\tau}{2} + \frac{D_2(q)}{V_0}, \tag{3.5}$$

where $D_2(q)$ is given by the second of Eq. (3.3). The solution after the reflection pulse is applied:

$$G(\tau) = -\frac{\tau}{2} + \frac{2D_2(q_m) - D_2(q)}{V_0}, \tag{3.6}$$

where $D_2(q_m)$ is given by the second of Eq. (3.3) with $q_m = (X_0)_m/R$ as the maximum relative excursion of a harmonic before the reflection pulse is applied. The solution for $R(\tau)$ for small times can be approximated to

$$R(\tau) = 1 - \frac{\tau^2}{4}, \tag{3.7}$$

as there is a small effect by $d_2(q)$ on R (refer Figure 2.2).

3.3.2 Speeds of a split cloud at different times

In a single reflection interferometer, the split clouds with initial velocities $\pm v_0$ are reflected by a laser pulse at $\tau = T/2$, where T is the interferometric cycle time. The

reflection laser pulse adds velocities of $\mp 2v_0$ to the clouds so that they now move with velocities $(v \mp 2v_0)$, v being the velocity of the clouds right before the reflection pulse is applied. A recombination pulse is applied to recombine the two clouds at time $\tau = T$. In this interferometer, the energy is conserved only in the period between the application of laser pulses.

The total energy of the split condensate in a trap in dimensionless variables is given by

$$\begin{aligned} E_T &= \frac{1}{2}\left(V + \frac{S}{10R}\right)^2 + \frac{G^2}{10R^2} + \frac{S^2}{175R^2} + \frac{1}{2}\left(X_0^2 + \frac{R^2}{5}\right) \\ &+ \frac{1}{10R}\left(1 + 10qd_1 + 2d_2\right). \end{aligned} \tag{3.8}$$

The details of the derivation of Eq. (3.8) can be found in Section 2.4.8. The normalizations of various parameters into dimensionless forms are given in Sections 2.2 and 2.3.2.

At time $\tau = 0$, $R = R_0 = 1$, $S = 0$, $G = 0$, $X_0 = 0$, $d_1 = 0$, and $d_2 = 1$. Making these substitutions, the total energy of the system right after the application of the splitting pulse,

$$E_T(\tau = 0) = \frac{1}{2}\left(V_0^2 + \frac{4}{5}\right). \tag{3.9}$$

When the two clouds just separate, $S = -1/(2V_0)$, $R \approx R_0$, $X_0 \approx R_0$ and $d_1 = 0 = d_2$. For small times, $G \sim \tau \sim 1/V_0$. Then from Eqs. (3.8) and (3.9) , the speed of the split clouds at separation

$$V(\tau \approx R_0/V_0) = V_0 - \frac{3}{10V_0}, \tag{3.10}$$

where we have neglected the terms of the order of V_0^{-2}.

The total energy of the system of the split clouds at $\tau = T/2$ (i.e., just before applying the reflection pulse) is given by

$$E_T(\tau = T/2) = \frac{1}{2}\left[V^2 + F(q,\tau)\right], \tag{3.11}$$

where

$$F(q,\tau) = \frac{VS}{5} + q^2 + \frac{2 + 10qd_1(q) + 2d_2(q)}{5}. \tag{3.12}$$

The terms containing G^2 and S^2 in the expression for energy (Eq. 3.8) were neglected in obtaining Eq. (3.11). For small values of q,

$$10qd_1(q) + 2d_2(q) \approx 2 - 10q^2,$$
$$D_3(q) \approx -35q^3,$$

and for $q \geq 1$, $d_1(q) = 0 = d_2(q)$ and $D_3(q) = -1/2$. For smaller times, the last of Eq. (3.1) gives $D_3(q) = VS$, where $D_3(q)$ is the polynomial function given by the last of Eq. (3.3). The speed V of a cloud right before reflection can be found by the energy conservation principle (Eqs. 3.8 and 3.9):

$$V^2 + F(q,\tau) = V_0^2 + \frac{4}{5}. \tag{3.13}$$

The energy after reflection will not be equal to the energy before reflection because the speed of a cloud changes from V to $(V - 2V_0)$ by the reflection pulse. The energy difference of the system after and before the application of the reflection pulse,

$$\begin{aligned}
\Delta E &= \frac{1}{2}\left[(V-2V_0)^2 + \frac{(V-2V_0)S}{5} - V^2 - \frac{VS}{5}\right] \\
&= \frac{1}{2}\left[-4(V-V_0)V_0 - \frac{2V_0 S(q_m)}{5}\right] \\
&= \frac{1}{2}\left[-\frac{8}{5} + 2F\left(q_m, \frac{T}{2}\right) - \frac{2D_3(q_m)}{5}\right],
\end{aligned} \tag{3.14}$$

where $V^2 - V_0^2 = 4/5 - F(q,\tau)$ at time $\tau = T/2$, which simplifies to $2V_0(V - V_0) \approx 4/5 - F(q_m, T/2)$ has been used to get the third equality. In Eq. (3.14), $q_m = (X_0)_m/R$ is the maximum relative excursion of a harmonic before the reflection pulse is applied.

If V is the velocity of the cloud right after the reflection pulse is applied, the energy of the system right after the application of the reflection pulse is onbtained

from Eq. (3.8),

$$\begin{aligned} E_T &= \frac{1}{2}\left[V^2 + \frac{D_3(q) - 2D_3(q_m)}{5} + q^2 + \frac{2 + 10qd_1 + 2d_2}{5}\right] \\ &= E_T(\tau = 0) + \Delta E\left(\tau = \frac{T}{2}\right). \end{aligned} \tag{3.15}$$

Using Eqs. (3.10), (3.14), and (3.15),

$$V^2 - V_0^2 = -\frac{4}{5} + 2F\left(q_m, \frac{T}{2}\right) - \frac{2D_3(q_m)}{5} - F(q, \tau). \tag{3.16}$$

Since the other quantities in the RHS of the Eq. (3.16) are fixed except $F(q, \tau)$, the equation for the V at recombination time T will be the same as given by the Eq. (3.16) with $F(q, \tau) = F(q, T)$:

$$V^2 - V_0^2 = -\frac{4}{5} + 2F\left(q_m, \frac{T}{2}\right) - \frac{2D_3(q_m)}{5} - F(q, T). \tag{3.17}$$

The Eq. (3.17) can be rewritten as

$$V^2 - V_0^2 = 2q_m^2 + \frac{20q_m d_1(q_m) + 4d_2(q_m)}{5} - \frac{D_3(q) - 2D_3(q_m)}{5} - q^2 - \frac{2 + 10qd_1 + 2d_2}{5}, \tag{3.18}$$

where V is the velocity of the cloud at the recombination time. For a perfect overlap of the two clouds at recombination, we set $q = 0$. The from Eq. (3.18) with $q_m = V_0 T/2$, the difference between the velocity of a cloud at recombination and its initial velocity,

$$\Delta V \approx \frac{V_0 T^2}{4}. \tag{3.19}$$

This velocity difference in dimensional variabes comes to be

$$\Delta v_D \approx \frac{v_0}{4}(\omega T_D)^2, \tag{3.20}$$

where v_0 is the initial velocity of a cloud, ω is the longitudinal trapping frequency, and T_D is the dimensional interferometric time.

3.4 Analysis of a double reflection interferometer

In a double reflection interferometer, the split clouds with initial velocities $\pm v_0$ are reflected by a laser pulse at times $\tau = T/4$ and $\tau = 3T/4$, where T is the interferometric cycle time. The first reflection laser pulse adds velocities of $\mp 2v_0$ to the clouds so that they now move with velocities $(v \mp 2v_0)$, v being the velocity of the clouds right before the first reflection pulse is applied. After the second reflection pulse, the veocities of the clouds become $(v \pm 2v_0)$ with v as their velocity right before the second reflection pulse is applied. A recombination pulse is applied to recombine the two clouds at time $\tau = T$. The energy is conserved only in the period between the application of laser pulses. We derive an expression for the difference in velocity of a cloud at recombination and the initial velocity by energy conservation principle. If the velocity of a cloud right before the first reflection pulse is V_1 and the excursion of the cloud is X_1, the expression for the total energy (from Eq. 3.8) of the cloud at this time

$$\begin{aligned} E_T(\tau = T/4_-) &= \frac{1}{2}\left(V_1 + \frac{S_1}{10R_1}\right)^2 + \frac{G_1^2}{10R_1^2} + \frac{S_1^2}{175R_1^2} \\ &+ \frac{1}{2}\left(X_1^2 + \frac{R_1^2}{5}\right) + \frac{f_1(q_1)}{10R_1}, \end{aligned} \tag{3.21}$$

where G_1, S_1, R_1 are the quadratic phase, cubic phase, and the radius of the cloud respectively at this time, and $f(q_1) = 1 + 10q_1d_1(q_1) + 2d_2(q_1)$. Since $S \propto V^{-1}$, we will neglect the terms containing S_1^2. This simplifies Eq. (3.21) to

$$E_T(\tau = T/4_-) = \frac{1}{2}\left(V_1^2 + \frac{V_1S_1}{5R_1}\right) + \frac{G_1^2}{10R_1^2} + \frac{1}{2}\left(X_1^2 + \frac{R_1^2}{5}\right) + \frac{f_1(q_1)}{10R_1}. \tag{3.22}$$

Substituting $V_1S_1 = D_3(q_1)$, (Eq. 3.22) can be written as

$$E_T(\tau = T/4_-) = \frac{1}{2}\left(V_1^2 + \frac{D_3(q_1)}{5R_1}\right) + \frac{G_1^2}{10R_1^2} + \frac{1}{2}\left(X_1^2 + \frac{R_1^2}{5}\right) + \frac{f_1(q_1)}{10R_1}. \tag{3.23}$$

The energy between the splitting and the first reflection pulse is conserved. Therefore, equating the energies at $\tau = T/4_-$ (Eq. 3.23) and $\tau = 0$ (Eq. 3.9) gives the velocity

of the cloud right before the application of the first reflection pulse as

$$V_{1-} = V_0 \left[1 + \frac{1}{2V_0^2}\left(\frac{4}{5} - \frac{D_3(q_1)}{5R_1} - \frac{G_1^2}{5R_1^2} - X_1^2 - \frac{R_1^2}{5} - \frac{f_1(q_1)}{5R_1}\right)\right]. \tag{3.24}$$

The first reflection pulse changes the velocity of the initially right-moving cloud by $-2V_0$. Therefore, the velocity of the cloud right after the first reflection is

$$V_{1+} = V_0 \left[-1 + \frac{1}{2V_0^2}\left(\frac{4}{5} - \frac{D_3(q_1)}{5R_1} - \frac{G_1^2}{5R_1^2} - X_1^2 - \frac{R_1^2}{5} - \frac{f_1(q_1)}{5R_1}\right)\right], \tag{3.25}$$

and the energy right after the first reflection,

$$\begin{aligned} E_T(\tau = T/4_+) &= \frac{1}{2}V_0^2 - \frac{4}{10} + \frac{1}{10R_1}\left(D_3(q) - D_3(q_1)\right) + \frac{G_1^2}{5R_1^2} + X_1^2 + \frac{1}{5}R_1^2 + \frac{f_1(q_1)}{5R_1} \\ &= \frac{1}{2}V_0^2 - \frac{2}{5} + \frac{G_1^2}{5R_1^2} + X_1^2 + \frac{1}{5}R_1^2 + \frac{f_1(q_1)}{5R_1}, \end{aligned} \tag{3.26}$$

where $D_3(q) = D_3(q_1)$ has been used because the reflection pulse is applied for a very short duration in comparison to the whole interferometric cycle time. We have neglected the terms multiplied by V_0^{-4} in evaluating the total energy because the terms containing this factor are much smaller than the other terms in the total energy.

The various parameters of the clouds after the first reflection pulse evolve with time but the total energy remains the same until the second reflection pulse is applied. Let X_2 be the excursion of the cloud and V_2 be its velocity right before the second reflection pulse is applied. The total energy of the clouds at this time,

$$\begin{aligned} E_T(\tau = 3T/4_-) &= \frac{1}{2}\left(V_2^2 + \frac{D_3(q_2) - 2D_3(q_1)}{5R_1}\right) + \frac{G_2^2}{10R_2^2} \\ &+ \frac{1}{2}\left(X_2^2 + \frac{R_2^2}{5}\right) + \frac{f_2(q_2)}{10R_2}. \end{aligned} \tag{3.27}$$

Equating the energies of the cloud at times $t = T/4_+$ (Eq. 3.26) and $\tau = 3T/4_-$ (Eq. 3.27), we get the velocity of the cloud right before the second pulse is applied as

$$\begin{aligned} V_{2-} &= V_0 \left[1 + \frac{1}{2V_0^2}\left\{-\frac{4}{5} + \frac{2}{5}\left(\frac{G_1^2}{R_1^2} - \frac{G_2^2}{2R_2^2}\right) + (2X_1^2 - X_2^2)\right.\right. \\ &+ \left.\left.\frac{1}{5}(2R_1^2 - R_2^2) + \frac{1}{5}\left(\frac{2f_1}{R_1} - \frac{f_2}{R_2}\right) - \frac{D_3(q_2) - 2D_3(q_1)}{5R_2}\right\}\right]. \end{aligned} \tag{3.28}$$

The velocity of the cloud right after the second reflection can be obtained by adding $+2V_0$ to V_2. But since V_2 itself is negative, the actual velocity of the cloud after reflection will be $(-V_2 + 2V_0)$. Therefore, the energy of the cloud after using the reflection pulse,

$$\begin{aligned} E_T(\tau = 3T/4_+) &= \frac{1}{2}V_0^2 + \frac{2}{5} - \frac{1}{5}\left(\frac{G_1^2}{R_1^2} - \frac{G_2^2}{R_2^2}\right) \\ &- (X_1^2 - X_2^2) - \frac{1}{5}(R_1^2 - R_2^2) - \frac{1}{5}\left(\frac{f_1}{R_1} - \frac{f_2}{R_2}\right). \end{aligned} \tag{3.29}$$

If V_T be the velocity at the time of recombination $\tau = T$, and assuming that the two clouds completely overlap at the center of the trap ($X_3 = 0$) at this time, the total energy of the cloud,

$$E_T(\tau = T) = \frac{1}{2}\left(V_T^2 + \frac{D_3(q_3)}{5R_T}\right) + \frac{G_3^2}{10R_T^2} + \frac{R_T^2}{10} + \frac{3}{10R_T}, \tag{3.30}$$

where R_T is the radius of the cloud at time $\tau = T$. Equating the right hand sides of Eqs. (3.29) and (3.30) gives the velocity at time T as,

$$\begin{aligned} V_T &= V_0 + \frac{1}{2V_0}\left[\frac{4}{5} - \frac{2}{5}\left(\frac{G_1^2}{R_1^2} - \frac{G_2^2}{R_2^2} + \frac{G_3^2}{2R_T^2}\right) - 2(X_1^2 - X_2^2)\right] \\ &+ \frac{1}{2V_0}\left[-\frac{2}{5}\left(R_1^2 - R_2^2 + \frac{1}{2}R_T^2\right) - \frac{2}{5}\left(\frac{f_1}{R_1} - \frac{f_2}{R_2}\right) - \frac{1}{5R_T}(D_3(q_3) + 3)\right]. \end{aligned} \tag{3.31}$$

For completely overlapped clouds at the time of recombination at the center of the trap, $D_3(q_3) = 0$ which gives,

$$\begin{aligned} V_T &= V_0 + \frac{1}{2V_0}\left[\frac{4}{5} - \frac{2}{5}\left(\frac{G_1^2}{R_1^2} - \frac{G_2^2}{R_2^2} + \frac{G_3^2}{2R_T^2}\right) - 2(X_1^2 - X_2^2)\right] \\ &+ \frac{1}{2V_0}\left[-\frac{2}{5}\left(R_1^2 - R_2^2 + \frac{1}{2}R_T^2\right) - \frac{2}{5}\left(\frac{f_1}{R_1} - \frac{f_2}{R_2}\right) - \frac{3}{5R_T}\right]. \end{aligned} \tag{3.32}$$

The difference in velocity at time T and initial velocity,

$$\begin{aligned} \Delta V &= \frac{1}{2V_0}\left[\frac{4}{5} - \frac{2}{5}\left(R_1^2 - R_2^2 + \frac{1}{2}R_T^2\right) - \frac{3}{5R_T} - 2(X_1^2 - X_2^2)\right] \\ &+ \frac{1}{2V_0}\left[-\frac{2}{5}\left(\frac{G_1^2}{R_1^2} - \frac{G_2^2}{R_2^2} + \frac{G_3^2}{2R_T^2}\right) - \frac{2}{5}\left(\frac{f_1}{R_1} - \frac{f_2}{R_2}\right)\right], \end{aligned} \tag{3.33}$$

where $\Delta V = V_T - V_0$. Rearranging the terms,

$$\begin{aligned}\Delta V &= \frac{2}{5V_0}\left[1 - \frac{1}{2}\left(R_1^2 - R_2^2 + \frac{1}{2}R_T^2\right) - \frac{3}{4R_T} - \frac{5}{2}(X_1^2 - X_2^2)\right. \\ &- \left.\frac{1}{2}\left(\frac{G_1^2}{R_1^2} - \frac{G_2^2}{R_2^2} + \frac{G_3^2}{2R_T^2}\right) - \frac{1}{2}\left(\frac{f_1}{R_1} - \frac{f_2}{R_2}\right)\right]. \end{aligned} \tag{3.34}$$

Employing approximations for R and G at smaller times (refer Eqs. 3.7 and 3.6),

$$\Delta V \approx -\frac{3T^2}{20V_0}, \tag{3.35}$$

where the contribution from the term containing $(X_1^2 - X_2^2)$ is negligible compared to the other terms and has been neglected. The velocity difference (Eq. 3.35) in dimensional form,

$$\Delta v_D \approx -\frac{3}{20}\frac{\omega^4 T_D^2 L_0^2}{v_0}. \tag{3.36}$$

The difference in the velocities obtained by a different technique in [46, 47],

$$\Delta v_D \approx -\frac{3}{16}\frac{\omega_D^4 T_D^2 R_D^2}{v_0}. \tag{3.37}$$

The parameters ω and L_0 in Eq. (3.36) are the same as the ω_D and R_D respectively in Eq. (3.37).

To compare the loss of contrast in the reflection interferometers with that of free oscillation interferometer, we need the difference in velocity at recombination time and initial velocity in a free oscillation interferometer. This can be obtained from Eq. (2.85) which results to

$$\Delta v_D \approx -\frac{1}{20}\frac{\omega^2 L_0^2}{v_0}. \tag{3.38}$$

3.5 Conclusions

We derived expressions for the differences in velocity of a split cloud at recombination and its initial velocity in single and double reflection interferometers by energy conservation principle and using the equations of motion derived from the expectation

values of various dynamical quantities. The expressions (Eqs. 3.20 and 3.36) agree very well with the analogous expressions in [45, 47] obtained by a different technique.

A comparison of the Eqs. (3.20), (3.36) and (3.38) shows that the difference in velocity at recombination and initial velocity of a cloud is much larger in a single reflection interferometer, less in double reflection interferometer, and much smaller in a free oscillation interferometer for a given trap frequency. Since this velocity difference is the main cause of the loss of contrast (see Section 2.5.9 for details), an increasingly improved contrast can be obtained in a double reflection and free oscillation interferometers compared to a single reflection interferometer.

Chapter 4

Conclusion and outlook

'A jug fills drop by drop.' - Buddha

4.1 Conclusion

We theoretically studied the dynamics of a split condensate in a harmonic oscillator trap and analyzed the operation of BEC-based atom Michelson interferometers with and without using reflection pulses. We investigated the effects of trap frequencies, nonlinearity caused by atom-atom interactions in the condensate and the velocity mismatch created by the reflection pulses on interferometry. Our results show that these factors are responsible for the loss of contrast of the interferometric fringes and set a theoretical limit of performance in the parameter space of the interferometers. The contrast of interferometric fringes in a free oscillation interferometer is higher than in the reflection interferometers. We have also shown that the contrast of the interferometric fringes in a double reflection interferometer is better than the contrast in a single reflection interferometer because of a symmetric motion of the split clouds in the double reflection geometry. Finally, we compared our results with the recent

experiments on BEC-based atom interferometers.

These interferometers have their limitations too. The interferometric cycle time can be controlled in the single and double reflection interferometers by controlling the time when the reflection pulses are applied. On the other hand, the interferometric cycle time in a free oscillation interferometer depends upon the longitudinal trap frequency. If the trap frequency is very weak, the split clouds spend more time in the arms of the interferometer and may suffer from an unwanted spatial phase gradient due to noise.

4.2 Future direction

A slight misalingnment of the splitting pulse will impart momentum components on the split clouds along radial dimension of the guide in addition to the momenta along the axis of the guide. In such a situation, the clouds will oscillate on a plane which gives a richer and more challenging dynamics with more dynamical quantities in the analysis of a free oscillation interferometer. The radial oscillations may contribute an increased loss of contrast of the interferometric fringes because the clouds oscillate several times radially depending upon the transverse trap frequencies before they return to the center of the trap. At the time of recombination, the clouds may overlap partially or they may even completely miss each other. For a full description of this situation, the one dimensional model has to be generalized to higher dimensions.

Bibliography

[1] I. Newton, *Opticks: OR, A Treatise of the Reflections, Refractions, Inflections, and Colours of Light* (William Innys, London, 1730).

[2] F. A. Jenkins and H. E. White, *Fundamentals of Optics* (McGraw-Hill Book Company, Inc., New York, 1950).

[3] E. Hecht, *Optics* (Pearson Education, Inc., San Franscisco, 2002).

[4] E. J. Post, "Sagnac effect," Rev. Mod. Phys. **39,** 475 (1967).

[5] C. J. Foot, *Atomic Physics* (Oxford University Press, Oxford, 2005).

[6] G. F. Missiroli, G. Pozzi, and U. Valdre, "Electron interferometry and interference elctron microscopy," J. Phys. E: Sci. Instrum. **14,** 649 (1981).

[7] A. H. Zewail and J. M. Thomas, *4D Electron Microscopy Imaging in Space and Time* (Imperial College Press, London, 2010).

[8] J. Chadwick, "Possible existence of a neutron," Nature **129,** 312 (1932).

[9] D. M. Greenberger, "The neutron interferometer as a device for illustrating the strange behavior of quantum systems," Rev. Mod. Phys. **55,** 875 (1983).

[10] N. F. Ramsey, *Molecular Beams* (Oxford University Press, Oxford, 1986).

[11] O. Carnal and J. Mlynek, "Youngs double-slit experiment with atoms: A simple atom interferometer," Phys. Rev. Lett. **66,** 2689 (1991).

[12] D. W. Keith, C. R. Ekstrom, Q. A. Turchette, and D. E. Pritchard, "An interferometer for atoms," Phys. Rev. Lett. **66,** 2693 (1991).

[13] W. D. Phillips, "Nobel Lecture: Laser cooling and trapping of neutral atoms," Rev. Mod. Phys. **70,** 721 (1998).

[14] M. Kasevich and S. Chu, "Atomic interferometry using stimulated Raman transitions," Phys. Rev. Lett. **67,** 181 (1991).

[15] A. D. Cronin, J. Schmiedmayer, and D. E. Pritchard, "Optics and interferometry with atoms and molecules," Rev. Mod. Phys. **81,** 1051 (2009).

[16] L. Pitaevskii and S. Stringari, *Bose-Einstein Condensation* (Oxford University Press, Oxford, 2003).

[17] M. H. Anderson, J. R. Ensher, M. R. Matthews, C. E. Wieman, , and E. A. Cornell, "Observation of Bose-Einstein Condensation in a Dilute Atomic Vapor," Science **269,** 198 (1995).

[18] K. B. Davis, M. O. Mewes, M. R. Andrews, N. J. van Druten, D. S. Durfee, D. M. Kurn, and W. Ketterle, "Bose-Einstein Condensation in a Gas of Sodium Atoms," Phys. Rev. Lett. **75,** 3969 (1995).

[19] C. C. Bradley, C. A. Sackett, J. J. Tollett, and R. G. Hulet, "Evidence of Bose-Einstein Condensation in an Atomic Gas with Attractive Interactions," Phys. Rev. Lett. **75,** 1687 (1995).

[20] C. J. Pethick and H. Smith, *Bose-Einstein Condensation in Dilute Gases* (Cambridge University Press, Cambridge, 2002).

[21] F. Dalfovo, S. Giorgini, L. P. Pitaevskii, and S. Stringari, "Theory of Bose-Einstein condensation in trapped gases," Rev. Mod. Phys. **71,** 463 (1999).

[22] A. J. Leggett, "Bose-Einstein condensation in the alkali gases: Some fundamental concepts," Rev. Mod. Phys. **73,** 307 (2001).

[23] K. Huang, *Statistical Mechanics* (John Wiley & Sons, Inc., New York, 1963).

[24] D. R. Tilley and J. Tilley, *Superfluidity and superconductivity* (Adam Hilger Ltd, Bristol, 1986).

[25] R. J. Donnelly, *Quantized vortices in helium II* (Cambridge University Press, Cambridge, 1991).

[26] I. Bloch, J. Dalibard, and W. Zwerger, "Many-body physics with ultracold gases," Rev. Mod. Phys. **80,** 885 (2008).

[27] E. Timmermans, "Superfluids and superfluid mixtures in atom traps," Contemporary Physics **42,** 1 (2001).

[28] R. Onofrio, C. Raman, J. M. Vogels, J. Abo-Shaeer, A. Chikkatur, and W. Ketterle, "Observation of Superfluid Flow in a Bose-Einstein Condensed Gas," Phys. Rev. Lett. **85,** 2228 (2000).

[29] J. R. Abo-Shaeer, C. Raman, J. M. Vogels, and W. Ketterle, "Observation of Vortex Lattices in Bose-Einstein Condensates," Science **292,** 476 (2001).

[30] J. Fortagh and C. Zimmermann, "Magnetic microtraps for ultracold atoms," Rev. Mod. Phys. **79,** 235 (2007).

[31] Y. J. Wang, D. Z. Anderson, V. Bright, E. A. Cornell, Q. Diot, T. Kishimoto, M. Prentiss, R. A. Saravanan, S. R. Segal, and S. Wu, "Atom Michelson interferom-

eter on a chip using a Bose-Einstein condensate," Phys. Rev. Lett. **94,** 090405 (2005).

[32] T. Schumm, S. Hofferberth, L. M. Andersson, S. Wildermuth, S. Groth, I. Bar-Joseph, J. Schmiedmayer, and P. Krger, "Matter-wave interferometry in a double well on an atom chip," Nat. Phys. **1,** 57 (2005).

[33] M. Horikoshi and K. Nakagawa, "Dephasing due to atom-atom interaction in a waveguide interferometer using a Bose-Einstein condensate," Phys. Rev. A **74,** 031602(R) (2006).

[34] D. M. Farkas, K. M. Hudek, E. A. Salim, S. R. Segal, M. B. Squires, and D. Z. Anderson, "A compact, transportable, microchip-based system for high repetition rate production of BoseEinstein condensates," Appl. Phys. Lett. **96,** 093102 (2010).

[35] P. R. Berman, *Atom Interferometry* (Academic Press, San Diego, 1997).

[36] A. Lenef, T. D. Hammond, E. T. Smith, M. S. Chapman, R. A. Rubenstein, and D. E. Pritchard, "Rotation Sensing with an Atom Interferometer," Phys. Rev. Lett. **78,** 760 (1997).

[37] B. Deissler, K. H. Hughes, J. H. T. Burke, and C. A. Sackett, "Measurement of the ac Stark shift with a guided matter-wave interferometer," Phys. Rev. A **77,** 031604(R) (2008).

[38] M. R. Andrews, C. G. Townsend, H.-J. Miesner, D. S. Durfee, D. M. Kurn, and W. Ketterle, "Observation of Interference Between Two Bose Condensates," Science **275,** 637 (1997).

[39] Y. Shin, M. Saba, T. A. Pasquini, W. Ketterle, D. E. Pritchard, and A. E. Leanhardt, "Atom Interferometry with Bose-Einstein Condensates in a Double-Well Potential," Phys. Rev. Lett. **92,** 050405 (2004).

[40] J. H. T. Burke, B. Deissler, K. H. Hughes, and C. A. Sackett, "Confinement effects in a guided-wave atom interferometer with millimeter-scale arm separation," Phys. Rev. A **78,** 023619 (2008).

[41] M. Horikoshi and K. Nakagawa, "Suppression of dephasing due to a trapping potential and atom-atom interactions in a trapped-condensate interferometer," Phys. Rev. Lett. **99,** 180401 (2007).

[42] O. Garcia, B. Deissler, K. J. Hughes, J. M. Reeves, and C. A. Sackett, "Bose-Einstein-condensate interferometer with macroscopic arm separation," Phys. Rev. A **74,** 031601(R) (2006).

[43] Y. Torii, Y. Suzuki, M. Kozuma, T. Sugiura, T. Kuga, L. Deng, and E. W. Hagley, "Mach-Zehnder Bragg interferometer for a Bose-Einstein condensate," Phys. Rev. A **61,** 041602(R) (2000).

[44] S. Wu, Y.-J. Wang, Q. Diot, and M. Prentiss, "Splitting matter waves using an optimized standing-wave light-pulse sequence," Phys. Rev. A **71,** 043602 (2005).

[45] J. A. Stickney, D. Z. Anderson, and A. A. Zozulya, "Increasing the coherence time of Bose-Einstein-condensate interferometers with optical control of dynamics," Phys. Rev. A **75,** 063603 (2007).

[46] J. A. Stickney, R. P. Kafle, D. Z. Anderson, and A. A. Zozulya, "Theoretical analysis of single- and double- reflection atom interfrometer in a weakly confining magnetic trap," Phys. Rev. A **77,** 043604 (2008).

[47] J. A. Stickney, "A theoretical analysis of Bose-Einstein condensate based beam-splitters, interferometers, and transistors," PhD dissertation (2007).

[48] S. R. Segal, Q. Diot, E. A. Cornell, A. A. Zozulya, and D. Z. Anderson, "Revealing buried information: Statistical processing techniques for ultracold-gas image analysis," Phys. Rev. A **81,** 053601 (2010).

[49] J. E. Simsarian, J. Denschlag, M. Edwards, C. W. Clark, L. Deng, E. W. Hagley, K. Helmerson, S. L. Rolston, and W. D. Phillips, "Imaging the Phase of an Evolving Bose-Einstein Condensate Wave Function," Phys. Rev. Lett. **85,** 2040 (2000).

[50] M. Olshanii and V. Dunjko, "Interferometry in dense nonlinear media and interaction-induced loss of contrast in microfabricated atom interferometers," arXiv.org:cond-mat/0505358 (2005).

[51] E. O. Ilo-Okeke and A. A. Zozulya, "Atomic population distribution in the output ports of cold-atom interferometers with optical splitting and recombination," Phys. Rev. A **82,** 053603 (2010).

[52] J. H. T. Burke and C. A. Sackett, "Scalable Bose-Einstein-condensate Sagnac interferometer in a linear trap," Phys. Rev. A **80,** 061603(R) (2009).

Appendix A

Published work

This appendix contains a reprint of the paper on *analysis of a free oscillation atom interferometer* published in Physical Review A.

Analysis of a free oscillation atom interferometer

Rudra P. Kafle,[1] Dana Z. Anderson,[2] and Alex A. Zozulya[1,*]

[1]*Department of Physics, Worcester Polytechnic Institute, 100 Institute Road, Worcester, Massachusetts 01609, USA*

[2]*Department of Physics and JILA, University of Colorado and National Institute of Standards and Technology, Boulder, Colorado 80309-0440, USA*

(Received 8 February 2011; published 27 September 2011)

We analyze a Bose-Einstein condensate (BEC)-based free oscillation atom Michelson interferometer in a weakly confining harmonic magnetic trap. A BEC at the center of the trap is split into two harmonics by a laser standing wave. The harmonics move in opposite directions with equal speeds and turn back under the influence of the trapping potential at their classical turning points. The harmonics are allowed to pass through each other and a recombination pulse is applied when they overlap at the end of a cycle after they return for the second time. We derive an expression for the contrast of the interferometric fringes and obtain the fundamental limit of performance of the interferometer in the parameter space.

DOI: 10.1103/PhysRevA.84.033639 PACS number(s): 03.75.Dg, 37.25.+k

I. INTRODUCTION

Atom interferometers using cold atoms or Bose-Einstein condensates (BECs) can have very high sensitivities in comparison to their optical counterparts [1], and can find potential applications in field-sensing and precision measurements [2]. Atom interferometers can be more versatile than the optical ones and have been used to measure acceleration [3], rotations [4], and dynamic polarizability of atoms [5].

The first atom-interferometry experiments with supersonic atomic beams were reported in Refs. [6,7]. The laser cooling techniques of neutral atoms developed in the 1980s [8] opened up the applications of cold atoms in atom interferometry. Atom interferometry with cold atoms by projecting them in a vertical direction was used to measure acceleration due to gravity [3].

After the experimental realizations of BECs in dilute atomic gases in the mid-1990s [9–11], the horizon of atom interferometry has broadened. The atoms in BECs have a very narrow momentum distribution and hence can be controlled and manipulated more easily than the thermal atoms by using light waves. Moreover, all atoms in BECs are in the same quantum state and hence BECs are excellent coherent sources of matter waves. The interference of two independent condensates was first reported in Ref. [12], in which two separate condensates were prepared in a double-well potential and allowed to interfere by switching off the potential and letting the condensates expand. Shin *et al.* [13] showed trapped atom interferometry with a condensate prepared in an optical single-well potential and then coherently split into two by deforming the single-well into a double-well potential. This, as well as several other experiments [1,14–16] on BEC-based atom interferometry, shows that condensates are good candidates for interferometric applications. BEC-based atom interferometers in Michelson geometry [1,17] and in Mach-Zehnder geometry [18,19] were realized recently.

The basic steps of guided atom interferometry are the following [20]: an atomic wave packet is split into two in a trap or a waveguide, the split wave packets are sent down two different paths, and recombined at the end of the interferometric cycle. For example, in a single-reflection atom Michelson interferometer, a BEC in a zero momentum state ψ_0 is split at time $\tau = 0$ by a laser standing wave into two harmonics ψ_+ and ψ_- [1,21,22]. The atoms in the ψ_+ harmonic absorb a photon from a laser beam with the momentum $\hbar k_l$ and re-emit into the beam with the momentum $-\hbar k_l$ (with k_l being the wave number of the laser), thus acquiring velocity $v_0 = 2\hbar k_l/M$, where M is the atomic mass. Similarly, an atom in the ψ_- harmonic acquires velocity $-v_0 = -2\hbar k_l/M$. At time $\tau = T/2$, where T is the interferometric cycle time, a reflection pulse is applied to reverse the momenta of the harmonics. At time $\tau = T$ the two harmonics are subject to the action of a recombination pulse. After recombination, in general, the atoms populate all three harmonics ψ_0 and $\psi_\pm$. The number of atoms in each harmonic depends on the relative phase acquired during the interferometric cycle and can be used to deduce this phase.

Loss of contrast in a single-reflection interferometer is primarily due to a coordinate-dependent phase acquired during the cycle. This phase is caused by the confining potential and the velocity mismatch due to reflection pulses. To overcome this drawback, a double-pass interferometer with reflection pulses was proposed and implemented in Ref. [17]. In this interferometer, each cloud travels in both arms of the interferometer before the clouds are finally recombined. Because of the symmetry in the paths followed by the two clouds, the coordinate-dependent phase is partially canceled. But the reflection pulses still introduce a velocity mismatch that limits the performance of the interferometer [22]. The performance can be further improved in the geometry of a free oscillation interferometer [15,23] that does not use the reflection pulses at all. In this geometry, the split clouds turn around in the confining potential at their classical turning points and pass through each other twice before they are finally recombined.

Both double-reflection and free oscillation interferometers are not suitable for measuring static environment like gravitational acceleration because both clouds accumulate equal environment-introduced phases during an interferometric cycle and hence the relative phase shift is zero. But they can be used for measuring environmental effects

*zozulya@wpi.edu

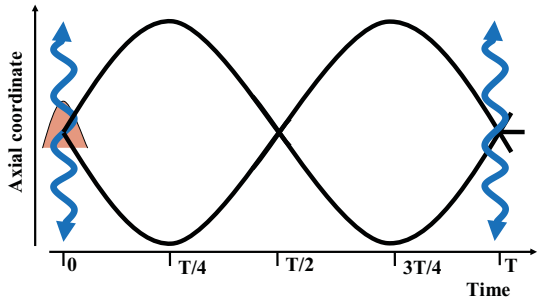

FIG. 1. (Color online) A schematic of a free oscillation interferometer.

that can be controlled in time. For example, Deissler *et al.* [5] measure the dynamic polarizability of ^{87}Rb atoms with a double-pass interferometer. Burke *et al.* [24] show that a double-pass interferometer can be used as a Sagnac interferometer to measure rotation using the Sagnac effect.

In this paper we theoretically analyze a free oscillation atom Michelson interferometer in the framework of a mean-field approach and obtain its limit of performance in the parameter space. This interferometer is schematically shown in Fig. 1. The solid lines are the paths followed by the two harmonics during an interferometric cycle and the vertical wavy lines represent the splitting and recombination laser pulses. The split condensates move in a weakly confining harmonic trap and are reflected from their classical turning points. They pass through each other, reach the maximum excursions in the opposite arms, and return again. The harmonics are recombined when they again overlap at the center of the trap. This interferometer has been experimentally realized in Refs. [15,23] and in a different (Mach-Zehnder) geometry in Ref. [16]. Horikoshi *et al.* [16] have shown that dephasing in this type of interferometer is suppressed. Nevertheless, there is still a fundamental limit on the performance of this geometry that is caused by the confining potential and the nonlinearity of the condensate, which is the subject of the present paper.

The rest of the paper is organized as follows: Sec. II formulates the analytical model used to describe the interferometer. The equations of motion for the split condensates are derived and analyzed in Sec. III. The limits of performance of the free oscillation interferometer are discussed in Sec. IV. The free oscillation interferometer is compared with the single- and double-reflection interferometers in Sec. V. Finally, conclusions are presented in Sec. VI.

II. ANALYTICAL MODEL

The results of this paper are obtained in the framework of a one-dimensional (1D) mean-field theory in Thomas-Fermi limit [25]. A 1D model is a good approximation to the experimental situation [1,15–17,19,23], where the BEC clouds are cigar shaped with the largest dimension along the weak guiding direction of the trap and are moving along the same direction.

Specifically, we describe the evolution of a BEC in a weakly confining parabolic potential of longitudinal frequency ω by the following dimensionless Gross-Pitaevskii equation (GPE):

$$i\frac{\partial}{\partial\tau}\psi(X,\tau)=\left[-\frac{\epsilon}{2}\frac{\partial^2}{\partial X^2}+\frac{1}{2\epsilon}X^2+g_{1D}|\psi(X,\tau)|^2\right]\psi(X,\tau). \tag{1}$$

The axial coordinate x is normalized to the initial longitudinal radius L_0 of the condensate: $X=x/L_0$. The dimensionless time τ is given by the relation $\tau=\omega t$, where ω is the longitudinal frequency of the weakly confining potential. The strength of interatomic interactions is described by the parameter $g_{1D}=2\omega_\perp a_s N/(\omega L_0)$ where a_s is the s-wave scattering length, N is the total number of atoms in the condensate, and $\omega_\perp$ is the trapping angular frequency in the tightly confined transverse dimensions. Finally, $\epsilon=(a_0/L_0)^2$, where $a_0=\sqrt{\hbar/(M\omega)}$ is the oscillator length along the longitudinal dimension. The wave function ψ has been normalized to 1. For details of derivation of Eq. (1) and its limits of applicability see [22].

The initial equilibrium size of the condensate in the Thomas-Fermi approximation [25] is given by

$$L_0=\left(\frac{3\hbar\omega_\perp a_s N}{M\omega^2}\right)^{1/3}. \tag{2}$$

The wave function ψ of the condensate after the splitting pulse is a superposition of two harmonics ψ_+ and ψ_-:

$$\psi=\frac{1}{\sqrt{2}}(\psi_++\psi_-). \tag{3}$$

The wave functions $\psi_\pm$ have been normalized to 1.

The densities $n_\pm$ and the phases $\phi_\pm$ of the harmonics ψ_+ and ψ_- defined by the relations $\psi_\pm=\sqrt{n_\pm}\exp(i\phi_\pm)$, are represented as

$$\begin{aligned} n_\pm&=\frac{3}{4R}\left[1-\left(\frac{X\mp X_0}{R}\right)^2\right],\\ \phi_\pm&=(\phi_0)_\pm+\frac{1}{\epsilon}\left[\pm V(X\mp X_0)+\frac{G}{2}\left(\frac{X\mp X_0}{R}\right)^2\right.\\ &\quad\left.\pm\frac{S}{6}\left(\frac{X\mp X_0}{R}\right)^3\right]. \end{aligned} \tag{4}$$

In Eq. (4), $\pm X_0(\tau)$ are the positions of the centers of the two harmonics and $R(\tau)=L/L_0$ is their dimensionless radius. Since the splitting pulses act for a very short period of time, the harmonics' shape and position immediately after splitting are equal to those of the initial BEC at rest [i.e., $X_0(0)=0$ and $R(0)=1$]. In the expression for the total phase of the split BECs [the second equation of Eq. (4)], the term $(\phi_0)_\pm$ is the phase accrued by the harmonics from the environment. The term $\pm V(X\mp X_0)$ is due to the motion of the two harmonics. The parameter $V(\tau)$ is the normalized speed v of the harmonics, that is, $V=v/(\omega L_0)$ with the initial value $V(0)=V_0=v_0/(\omega L_0)$. The quadratic term proportional to G appears because of dispersion of the harmonics. The cubic term proportional to S is due to atom-atom interactions in the condensate. The quadratic and cubic phases are initially zero, $G(0)=S(0)=0$ and evolve with time when the harmonics start propagating. The parabolic form of the density of the

BEC clouds $n_\pm$ in Eq. (4) implies the Thomas-Fermi limit, when the second derivative of the densities $n_\pm$ in Eq. (1) is neglected.

The Gross-Pitaevskii equation (1), with the form of the density and phase of the two BEC clouds given by Eq. (4), has been previously investigated under various approximations both analytically and numerically in [15,22,26,27]. In particular, the authors of Refs. [22,27] derived the set of coupled ordinary differential equations for the parameters $R(\tau)$, $X_0(\tau)$, $V(\tau)$, $G(\tau)$, $S(\tau)$, entering the expressions for the density and the phase of the BEC clouds given by Eq. (4) (notations of Refs. [22,27] are slightly different from those of the present paper). Validity of the analytical model has been confirmed by comparing solutions of these equations to the results following from direct numerical solution of the Gross-Pitaevskii equation (1). The derivation of equations in Refs. [22,27] has been based on representing the density and phase of the two BEC clouds (4) in terms of a truncated set of Legendre polynomials. In this paper we derive the set of equations analogous to that of Refs. [22,27] by analyzing equations of motion for the quantum-mechanical expectation values associated with the parameters $R(\tau)$, $X_0(\tau)$, $V(\tau)$, $G(\tau)$, and $S(\tau)$. This approach streamlines the derivation and allows for a greater insight into the physics. Additionally, it has the energy conservation law explicitly built in the formalism, greatly assisting further analysis. Finally, the new approach is more readily generalizable to two- or three-dimensional case. The set of derived equations is used to analyze the geometry of the free oscillation atom interferometer.

III. DYNAMICS OF THE SPLIT CONDENSATES

A. Equations of motion

The time evolution of the expectation value $\langle\hat{A}\rangle = \langle\psi|\hat{A}|\psi\rangle = \int \psi^* \hat{A}\psi dx$ of a quantum mechanical operator $\hat{A}$ is governed by the equation

$$\frac{d}{d\tau}\langle\hat{A}\rangle = i\langle\psi|[\hat{H},\hat{A}]|\psi\rangle, \tag{5}$$

where $\hat{H}$ is the Hamiltonian of the system and $[\hat{H},\hat{A}] = \hat{H}\hat{A} - \hat{A}\hat{H}$ is the commutator. The Hamiltonians of the two BEC clouds after the splitting are given by the relation

$$H_\pm = \frac{\epsilon}{2}P^2 + \frac{1}{2\epsilon}X^2 + \frac{1}{2}g_{1D}(n_\pm + 2n_\mp). \tag{6}$$

The expectation values of the coordinate X, that is, $\langle\psi|X|\psi\rangle$ and momentum P, that is, $\langle\psi|P|\psi\rangle$, evaluated with respect to the wave function ψ_+, are

$$\begin{aligned}\langle X\rangle &= X_0,\\ \langle P\rangle &= V + \frac{S}{10R}.\end{aligned} \tag{7}$$

Similarly, the expectation values of X^2, P^2, n_+, and n_- are

$$\begin{aligned}\langle X^2\rangle &= X_0^2 + \frac{R^2}{5},\\ \langle P^2\rangle &= \left(V + \frac{S}{10R}\right)^2 + \frac{G^2}{5R^2} + \frac{2S^2}{175R^2},\\ \langle n_+\rangle &= \frac{3}{5R},\\ \langle n_-\rangle &= \frac{3}{5R}(5qd_1 + d_2),\end{aligned} \tag{8}$$

where the functions d_i are defined by the relations (we shall need d_3 slightly later)

$$\begin{aligned}d_1(q) &= q(|q|-1)^2(|q|+2)\theta(|q|<1),\\ d_2(q) &= (|q|-1)^2(-6|q|^3 - 12|q|^2 + 2|q| + 1)\theta(|q|<1),\\ d_3(q) &= 35q|q|(|q|-1)^2(2|q|^2 + 4|q| - 3)\theta(|q|<1).\end{aligned} \tag{9}$$

Parameter $q = X_0/R$ in Eq. (9) is the relative position of the center of mass of a harmonic. The θ function in Eq. (9) is equal to one if its argument is a logical true and zero if it is a logical false. These functions arise because of the interatomic interactions between the two harmonics. Therefore, they are nonzero only when the harmonics are overlapping.

Using expectation values given by Eqs. (7) and (8) and evaluating their dynamics with the help of Eq. (5), results in a set of first-order differential equations describing the dynamics of the split condensates:

$$\begin{aligned}R_\tau &= \frac{G}{R},\\ G_\tau &= \frac{G^2}{R^2} - R^2\left(1 - \frac{1}{2R^3}\right) + \frac{1}{R}d_2(q),\\ (X_0)_\tau &= V + \frac{S}{10R},\\ \left(V + \frac{S}{10R}\right)_\tau &= -X_0 + \frac{d_1(q)}{R^2},\\ S_\tau &= \frac{d_3(q)}{R},\end{aligned} \tag{10}$$

where A_τ represents the derivative of the function A with respect to time.

In deriving the equations of motion Eq. (10), ϵ and V_0^{-1} were used as smallness parameters and terms of the order of ϵ^2 and V_0^{-2} have been neglected. This can be justified by the following estimate. For a BEC of ^{87}Rb atoms, $v_0 = 11.7$ mm/s. For the longitudinal angular frequency $\omega = 2\pi \times 4.1$ Hz, the angular frequency in the transverse dimensions $\omega_\perp = 2\pi \times 80$ Hz [23], and the number of atoms in the condensate $N = 10^4$ [1], the equilibrium size of a condensate L_0 given by Eq. (2) is approximately 40 μm. For these parameters, the inverse of the dimensionless initial speed V_0 of the harmonics is $V_0^{-1} \approx 0.09$ and $\epsilon \approx 0.018$.

Finally, analysis of Eq. (10) requires evaluation of functions $D_i(q) = \int_0^q d_i(x)dx$, which are integrals of the functions $d_i(q)$, with respect to q:

$$\begin{aligned}D_1(q) &= \tfrac{1}{5}q^2(|q|^3 - 5|q| + 5),\\ D_2(q) &= -q(|q|-1)^3(q^2 + 3|q| + 1),\\ D_3(q) &= \tfrac{1}{2}|q|^3\left(20q^4 - 126q^2 + 175|q| - 70\right).\end{aligned} \tag{11}$$

Expressions for the functions $D_i(q)$ given by Eq. (11) are valid in the region $|q| < 1$. For $|q| \geqslant 1$, the functions $D_i(q)$ are constant and equal to their boundary values : $D_1(\pm 1) = 1/5$, $D_2(\pm 1) = 0$, and $D_3(\pm 1) = -1/2$.

B. Evolution of the radius and the quadratic phase

Time dependence of the radius $R(\tau)$ and the quadratic phase $G(\tau)$ can be obtained by solving the first two equations of Eq. (10). The contribution from the term with $d_2(q)$ in the equation for G_τ can be neglected and these equations reduce to

$$R_{\tau\tau} = -R + \frac{1}{2R^2}. \tag{12}$$

Integrating Eq. (12) with initial conditions $R(0) = 1$ and $R_\tau(0) = 0$ yields

$$R_\tau = \pm\sqrt{\frac{(1-R)(R^2+R-1)}{R}}. \tag{13}$$

The first of Eq. (10) then gives

$$G(\tau) = \pm\sqrt{R(1-R)(R^2+R-1)}. \tag{14}$$

The analytic solution to Eq. (13) can be obtained in terms of elliptic functions. It is important to notice that Eq. (13) for R [and, thus, Eq. (14) for G] is "universal", that is, independent of the trap frequencies, number of atoms in the condensate, etc., and needs to be solved only once. Figure 2 shows the time evolution of R and G for a full trap period obtained by solving the first two of Eq. (10) numerically. The small kinks in the plot of G during splitting, at recombination, and when the harmonics pass through each other, are due to mutual interaction between the two harmonics at overlap (the term with d_2 in equation for G_τ). Figure 2 shows that the neglect of this term in obtaining Eq. (13) is an excellent approximation. It is interesting to note that the period of the oscillations of the radius is about 60% of the trap period. The quadratic phase G has the same period as R. In our analysis we shall need the values of R and G only at the time of recombination $\tau = 2\pi$: $R(2\pi) \approx 0.81$ and $G(2\pi) \approx 0.27$.

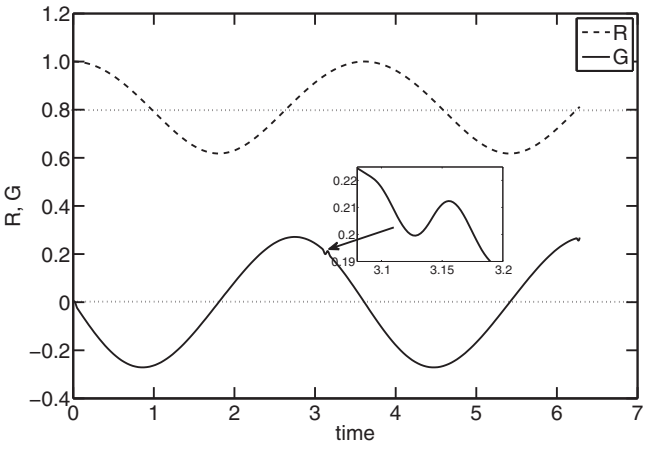

FIG. 2. Time evolution of the dimensionless radius R of a harmonic and the quadratic phase G (rad) for a trap period. The horizontal axis is dimensionless time from 0 to 2π. The inset shows the effect of interatomic interactions on G when the two harmonics pass through each other.

C. Evolution of the cubic phase

Evolution of the cubic phase $S(q)$ is governed by the last of Eq. (10). The cubic phase changes only when the harmonics overlap because, otherwise, the function $d_3(q)$ in Eq. (9) is zero. Integration of Eq. (10) yields

$$S(q) = \int_0^\tau d\tau' \frac{d_3(q)}{R} = \int_0^q dq \frac{d_3(q)}{R}\frac{d\tau}{dq} \approx \frac{D_3(q)}{V_0}, \tag{15}$$

because in the region of overlap $dq/d\tau \approx \pm V_0/R$ and $S(0) = 0$. The function $D_3(q)$ is given by Eq. (11). After the first separation of the harmonics, the value of S outside the overlap region is

$$S(1) = -\frac{1}{2V_0}, \tag{16}$$

because $D_3(1) = -1/2$. The difference between the values of S before and after the passage of the harmonics through each other around midcycle $\tau \approx T/2$ is zero, since its calculation involves integration of the odd function $d_3(q)$ from $q = 1$ to $q = -1$. Finally, near the end of the cycle

$$S(q) - S(-1) = \frac{1}{V_0}\left[D_3(q) - D_3(-1)\right]. \tag{17}$$

Combining Eqs. (16) and (17), the value of S near the end of the cycle

$$S(\tau \approx 2\pi) = \frac{D_3(q)}{V_0} \approx -\frac{35|q|^3}{V_0} \tag{18}$$

in the lowest order of $|q|$.

Figure 3 shows the evolution of S with time. It is zero initially and grows to a negative peak once the two harmonics start moving away from each other. After the harmonics completely separate, the value of S remains constant at its boundary value. The inset in Fig. 3 shows the evolution of S when the two harmonics pass through each other.

D. Energy of the system

The total energy E of the condensate is obtained by evaluating the expectation value of the Hamiltonian $\langle\psi|H|\psi\rangle$ with respect to the total wave function ψ of the split

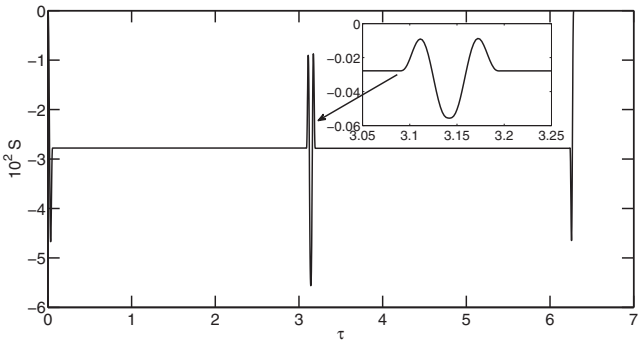

FIG. 3. Time evolution of the cubic phase S (rad). The horizontal axis is dimensionless time τ from 0 to 2π. The cubic phase develops only when the clouds overlap during splitting, when they pass through each other, and when they recombine. The inset shows the evolution of S when the clouds pass through each other.

condensates Eq. (3). This quantity can be represented as the sum of the three terms:

$$E = E_K + E_P + E_N, \tag{19}$$

with

$$E_K = \frac{1}{2}\left(V + \frac{S}{10R}\right)^2 + \frac{G^2}{10R^2},$$
$$E_P = \frac{1}{2}\left(X_0^2 + \frac{R^2}{5}\right),$$
$$E_N = \frac{(1 + 10qd_1 + 2d_2)}{10R},$$

where the d functions are given by Eq. (9). The term E_K in Eq. (19) is the kinetic energy of the system. It depends upon the speed of the clouds, the quadratic and the cubic phases. The kinetic energy right after splitting is proportional to V_0^2 but, when the clouds evolve with time, the quadratic and the cubic phases develop and the kinetic energy has terms containing speed as well as these phases. The term E_P is the potential energy of the clouds. This energy is equal to the sum of the potential energy of the condensate in the trap caused by its finite size, and the potential energy due to the displacement of the center of mass of each cloud after splitting. Due to its finite size, a cloud has nonzero potential energy even when it is at the bottom of the trap. Finally, the term E_N is nonlinear energy due to atom-atom interactions in the condensate.

During the interferometric time between the splitting and recombination pulse, the total energy of the system is conserved.

E. Wave function at recombination

The harmonics are recombined by using a recombination pulse at the end of the interferometric cycle time T. Since we are considering the case of $(\phi_0)_\pm = 0$ in Eq. (4), the recombination pulse, in the ideal situation, should recombine the two harmonics into one at rest. But, because of the spatially dependent phases accumulated during the interferometric cycle, there will be three harmonics in the output ports—one at rest and two moving in opposite directions [22]. The wave function for the zeroth order harmonic at recombination is given by the expression

$$\psi_0(\xi,q) = \sqrt{n(\xi)}\cos\phi(\xi,q), \tag{20}$$

where the spatial relative phase across a harmonic is

$$\phi(\xi,q) = \Delta K(q)\xi + \Gamma(q)\xi^3. \tag{21}$$

The strengths of the linear and cubic phases as functions of q is given by the relations

$$\Delta K(q) = \frac{R_T}{\epsilon}\left(V_T - V_0 - \frac{G_T}{R_T}q + \frac{S_T}{2R_T}q^2\right),$$
$$\Gamma(q) = \frac{S_T}{6\epsilon}, \tag{22}$$

where R_T, V_T, G_T, and S_T are evaluated at time T. In Eqs. (20) and (21), $\xi = X/R_T$ is the normalized coordinate and $q = X_0/R_T$ is the normalized position of the center of mass. We have neglected a small degree of incomplete overlap in the densities, but have taken it into account in phases.

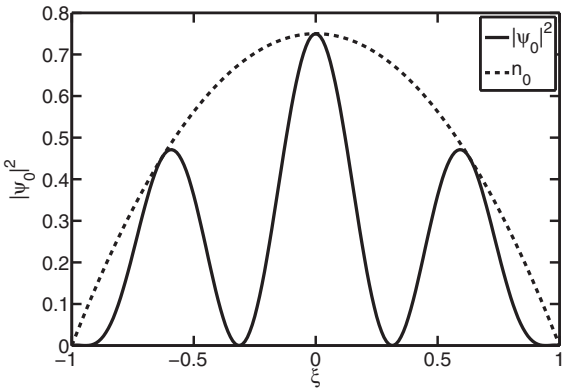

FIG. 4. The probability density $|\psi_0|^2$ vs the coordinate ξ for $\Delta K = 5$ and $\Gamma = 0$. The probability density oscillates several times under its envelope that reduces the contrast of the interference fringes.

IV. FRINGE CONTRAST AND LIMITS OF PERFORMANCE

The population in the zeroth order harmonic N_0 is given by the expression

$$N_0 = N_{\rm tot}\int |\psi_0(\xi,q)|^2 d\xi, \tag{23}$$

where ψ_0 is defined by Eq. (20). In the ideal case $\Delta K = \Gamma = 0$, the contrast of the interference fringes $V = 2N_0/N_{\rm tot} - 1$ should be equal to one, but the coordinate-dependent phase results in a decrease of the contrast. The physical reason for this decrease is explained by Fig. 4. When the coordinate-dependent phase $\phi(\xi,q)$ becomes large, the density profile undergoes several oscillations between its maximum value [given by the envelope $n(\xi)$] and zero. In this limit, the relative population in the zero momentum state after recombination $N_0/N_{\rm tot} = \int d\xi |\psi_0(\xi)|^2$ approaches $1/2$, and the contrast $V = [2(N_0/N_{\rm tot}) - 1]$ goes to zero.

The contrast of the fringes for small values of ΔK and Γ can be expressed as

$$V = 1 - \tfrac{2}{5}\left[(\Delta K)^2 + \tfrac{6}{7}\Delta K\Gamma + \tfrac{5}{21}\Gamma^2\right]. \tag{24}$$

Stickney *et al.* [27] noticed that the best contrast does not necessarily correspond to the complete overlap of the BEC clouds ($q = 0$) and sometimes can be improved by slightly changing the recombination time (or, equivalently, the value of q). We shall evaluate the limits of performance of the interferometer by minimizing the bracketed quantity on the right-hand side of Eq. (24) with respect to q and setting the result (somewhat arbitrarily) to 0.5.

The velocity V_T of the cloud at recombination time in the expression for ΔK given by Eq. (22) can be obtained by equating the total energy of the clouds at recombination time T to their total energy right after splitting ($\tau = 0$) because the total energy of the system is constant. From Eq. (19), the total energy of the system at time $\tau = 0$

$$E(0) = \tfrac{1}{2}\left(V_0^2 + \tfrac{4}{5}\right), \tag{25}$$

and the total energy at recombination time T

$$E(T) = \frac{V_T^2}{2} + \frac{G_T^2}{10R_T^2} + \frac{R_T^2}{10} + \frac{3}{10R_T}. \quad (26)$$

Equating the right-hand sides of Eqs. (25) and (26) gives

$$V_T - V_0 \approx -\frac{1}{2V_0}\left(\frac{G_T^2}{5R_T^2} + \frac{R_T^2}{5} + \frac{3}{5R_T} - \frac{4}{5}\right), \quad (27)$$

where V_T is the velocity of the harmonic right before the recombination pulse. By substituting $(V_T - V_0)$ from Eq. (27) into the first equation of Eq. (22), one gets

$$\Delta K(q) = -\frac{1}{\epsilon}\left(\frac{0.04}{V_0} + 0.27q\right), \quad (28)$$

where $q = X_0/R_T$ is the relative position of the center of mass of the ψ_+ harmonic. To get ΔK in the form given by Eq. (28), we used $R_0 = 1$, $R_T = 0.81$, and $G_T \approx 0.27$. Similarly, from the second equation of Eqs. (22) and (18),

$$\Gamma(q) = -\frac{35}{6\epsilon V_0}|q|^3. \quad (29)$$

Minimizing the bracketed quantity in the right-hand side of Eq. (24) with respect to q and requiring $V \geqslant 1/2$ results in an inequality

$$\frac{0.01}{\epsilon V_0^4} \leqslant 1 \quad (30)$$

that gives a working region in the parameter space of the interferometer. The inequality (30) can be expressed in terms of the dimensional experimental parameters as follows:

$$\left(\frac{\hbar\omega_\perp^2\omega a_s^2}{10Mv_0^4}\right)^{1/2} N \leqslant 1, \quad (31)$$

where N is the number of atoms in the trap of axial angular frequency ω and the transverse frequency $\omega_\perp$. This inequality gives a fundamental limit on performance of a guided BEC-based free oscillation interferometer in Michelson-type geometry. The second fundamental limit is due to phase diffusion, which cannot be described in the mean-field approach. In addition, there can be technical limitations like the noise (caused by vibrations), misalignment of the splitting laser pulse, etc.

Figure 5 shows the working region of a free oscillation interferometer for a transverse trapping frequency $\omega_\perp = 2\pi \times 80$ Hz. In the region below the boundary line [which has been obtained taking the equality sign in Eq. (31)] the interferometric contrast exceeds 50%. The maximum number of atoms corresponding to the boundary region for a given trap can be read directly from the graph. For example, for $\omega = 2\pi \times 4.1$ Hz, $N \approx 10^6$ and the interferometric cycle time is 244 ms (the trap period).

V. DISCUSSION OF SINGLE- AND DOUBLE-REFLECTION GEOMETRIES

In this section we briefly rederive results of the analysis of the single- and double-reflection atom Michelson interferometers [22,27] and compare their performance with that of

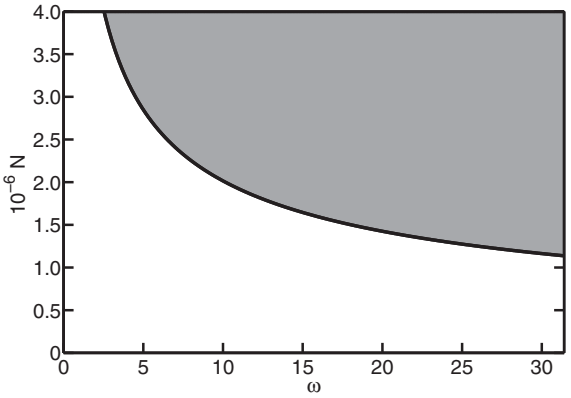

FIG. 5. Working region in parameter space of a free oscillation interferometer, with the longitudinal trap frequency ω (rad/s) and the total number of atoms N in the condensate. The interferometer works in the unshaded region and does not work in the shaded region.

the free oscillation interferometer. In a single-reflection atom Michelson interferometer, a BEC sitting at the bottom of a weakly confining harmonic trap is split into two harmonics, which move in opposite directions with the velocities $\pm V_0$. At time $\tau = T/2$ where T is the interferometric cycle time, a reflection pulse is applied, which adds velocities of $\mp 2V_0$ to the harmonics so that the ψ_+ harmonic now moves with a velocity $(V_+ - 2V_0)$ and the ψ_- harmonic moves with a velocity $(V_- + 2V_0)$, where $V_\pm = \pm V$ are the velocities of the two harmonics right before the first reflection pulse is applied. A recombination pulse, identical to the splitting pulse is used to recombine the two harmonics at time $\tau = T$.

The total energy of the system is given by Eq. (19). Unlike in the case of a free oscillation interferometer, the energy is not conserved for a complete cycle because of the reflection pulses, but remains constant between them. In this case, the velocity of the harmonics at the time of recombination can be calculated from Eq. (19) taking into account the momentum kick given to the harmonics by the reflection pulse. The difference between the final speed of the ψ_+ harmonic and its initial speed $\Delta V = (V_T - V_0)$ in the dimensionless variables turns out to be

$$\Delta V \approx \frac{V_0 T^2}{4}. \quad (32)$$

In deriving Eqs. (32), (13), and (14) have been solved to the lowest order in τ yielding $G \approx -\tau/2$ and $R \approx 1 - \tau^2/4$, because the duration of the interferometric cycle in this case is much less than the full period of oscillation in the trap. The dimensional version of Eq. (32) reads

$$\Delta v_D \approx \frac{v_0}{4}(\omega T_D)^2, \quad (33)$$

where $v_0 = 2\hbar k_l/M$, L_0 is the equilibrium size of the condensate, and T_D is the dimensional time for the interferometric cycle. Relation (33) coincides with the analogous relation Eq. (24) in Ref. [27] obtained by a different technique.

In a double-reflection interferometer, two reflection pulses are applied at times $\tau = T/4$ and $\tau = 3T/4$ before the

recombination pulse is applied at the end of the interferometric cycle time $\tau = T$. Using the procedure analogous to that described above, we calculate the difference between the velocity of the ψ_+ harmonic at recombination (V_T) and initial velocity (V_0) to be equal to

$$\Delta V \approx -\frac{3T^2}{20V_0}, \tag{34}$$

or, in dimensional variables,

$$\Delta v_D \approx -\frac{3}{20}\frac{\omega^4 T_D^2 L_0^2}{v_0}. \tag{35}$$

This expression matches with the analogous relation Eq. (43) in Ref. [27].

Equations (32) and (34) have been obtained in the limit when the clouds have zero spatial overlap at the time of application of the reflection pulses.

To compare the performances of the single-, double-reflection, and free oscillation interferometers, it is enough to compare the differences between the velocity of the ψ_+ harmonic at recombination (V_T) and its initial velocity (V_0) in the three geometries. For a free oscillation interferometer, $(V_T - V_0)$ given by Eq. (27) becomes

$$\Delta v_D \approx -\frac{1}{20}\frac{\omega^2 L_0^2}{v_0} \tag{36}$$

in dimensional variables. A comparison of Eqs. (33), (35), and (36) shows that the difference in velocities at recombination and initial velocity of a cloud is much larger in a single-reflection interferometer, less in double-reflection interferometer, and much smaller in a free oscillation interferometer for a given trap frequency. Since this velocity difference is the main cause of the loss of contrast [cf. Eqs. (22) and (24)], an increasingly improved contrast can be obtained in a double-reflection and free oscillation interferometers compared to a single-reflection interferometer.

VI. CONCLUSIONS

In this paper we analyzed the operation of a BEC-based free oscillation interferometer with optical splitting and recombination of the BEC clouds. Our one-dimensional (1D) analytical model is based on the mean-field approximation in the Thomas-fermi limit. From the 1D Gross-Pitaevskii equation we derive a closed set of ordinary differential equations for the parameters describing the shape of the density envelope and the spatially varying phase of the BEC clouds. The derivation is based on the equations of motion for the quantum-mechanical expectation values associated with these parameters. The main result of the paper is Eq. (31), which gives the working region of the interferometer in the parameter space and shows how the performance of the interferometer depends on different parameters of the experiment such as the number of particles, longitudinal and transverse frequencies of the trap, and the velocity imparted by the splitting laser pulses. According to our analysis, the reason for the loss of the coherence in a free oscillation interferometer is oscillations of the density envelopes of the clouds with a period different from the longitudinal period of the trap.

The analysis of the paper does not include effects beyond the mean-field approximation such as finite-temperature phase fluctuations along the length of the elongated BEC clouds and phase diffusion. Reference [27] discussed the importance of the phase fluctuations and concluded that they are negligible for the parameters of the recent experiments [1,15,17,23]. The phase diffusion, specifically in the context of atom interferometers with the optical splitting and recombination of the clouds, has been recently analyzed in [28]. Results of this analysis, applied to the case of a free oscillation interferometer, predict that the region of good performance is given by the inequality

$$\left(\frac{a_s}{\bar{a}}\right)^{2/5}\left(\frac{2\pi\bar{\omega}}{\omega}\right)N^{-1/10} \leqslant 1, \tag{37}$$

where $\bar{\omega} = (\omega_\perp^2\omega)^{1/3}$ and $\bar{a} = \sqrt{\hbar/(M\bar{\omega})}$.

The model of Ref. [28] goes beyond the mean-field approximation by accounting for the mode-entangled nature of the two BEC clouds after the splitting, but does not account for the development of spatially varying phases caused by atom-atom interaction during the propagation, as opposed to the present paper. Thus, the physics behind Eqs. (31) and (37) is complementary, and both these inequalities have to be evaluated and their values compared for any particular experiment.

The relative importance of the effects due to spatially varying phases caused by atom-atom interactions and the phase diffusion is given by the left-hand sides of Eqs. (31) and (37), respectively. The left-hand side of Eq. (31) for the parameters of the experiments by Burke *et al*. [15] and Horikoshi *et al*. [16] is much less than one, and equals about 0.8 in the experiments by Segal *et al*. [23]. The left-hand side of Eq. (37) for Ref. [15] is small as compared to one and equals about 0.65 and 1.0 for Refs. [16] and [23], respectively. This shows that the phase diffusion could be partially responsible for the degradation of coherence in [16] and that both the effects discussed in this paper and the phase diffusion could be at least partially responsible for the loss of contrast in the experiments [23]. The authors of Refs. [15,16,23] also list vibrations as a cause for the degradation of the coherence.

In the experiments discussed in the paper, the frequency of the trap along the guiding direction is much less than those along the transverse directions. The BEC clouds are cigar shaped with the largest dimension along the weak guiding direction of the trap and are moving along the same direction. This is the reason why a 1D theory is a good approximation to the experimental situation. A possible slight misalignment of the optical splitting pulses can result in a more complicated 2D or 3D motion of the BEC clouds and their rotations. Analysis of such dynamics requires generalization of the 1D model of the present paper to higher dimensions.

ACKNOWLEDGMENTS

This work was partially supported by the Defense Advanced Research Projects Agency (Grant No. W911NF-04-1-0043).

[1] Y. J. Wang, D. Z. Anderson, V. M. Bright, E. A. Cornell, Q. Diot, T. Kishimoto, M. Prentiss, R. A. Saravanan, S. R. Segal, and S. Wu, Phys. Rev. Lett. **94**, 090405 (2005).
[2] P. R. Berman, ed., *Atom Interferometry* (Academic Press, San Diego, 1997).
[3] M. Kasevich and S. Chu, Phys. Rev. Lett. **67**, 181 (1991).
[4] A. Lenef, T. D. Hammond, E. T. Smith, M. S. Chapman, R. A. Rubenstein, and D. E. Pritchard, Phys. Rev. Lett. **78**, 760 (1997).
[5] B. Deissler, K. J. Hughes, J. H. T. Burke, and C. A. Sackett, Phys. Rev. A **77**, 031604(R) (2008).
[6] O. Carnal and J. Mlynek, Phys. Rev. Lett. **66**, 2689 (1991).
[7] D. W. Keith, C. R. Ekstrom, Q. A. Turchette, and D. E. Pritchard, Phys. Rev. Lett. **66**, 2693 (1991).
[8] W. D. Phillips, Rev. Mod. Phys. **70**, 721 (1998).
[9] M. H. Anderson, J. R. Ensher, M. R. Matthews, C. E. Wieman, and E. A. Cornell, Science **269**, 198 (1995).
[10] K. B. Davis, M.-O. Mewes, M. R. Andrews, N. J. van Druten, D. S. Durfee, D. M. Kurn, and W. Ketterle, Phys. Rev. Lett. **75**, 3969 (1995).
[11] C. C. Bradley, C. A. Sackett, J. J. Tollett, and R. G. Hulet, Phys. Rev. Lett. **75**, 1687 (1995).
[12] M. R. Andrews, C. G. Townsend, H.-J. Miesner, D. S. Durfee, D. M. Kurn, and W. Ketterle, Science **275**, 637 (1997).
[13] Y. Shin, M. Saba, T. A. Pasquini, W. Ketterle, D. E. Pritchard, and A. E. Leanhardt, Phys. Rev. Lett. **92**, 050405 (2004).
[14] T. Schumm, S. Hofferberth, L. M. Andersson, S. Wildermuth, S. Groth, I. Bar-Joseph, J. Schmiedmayer, and P. Krüger, Nat. Phys. **1**, 57 (2005).
[15] J. H. T. Burke, B. Deissler, K. J. Hughes, and C. A. Sackett, Phys. Rev. A **78**, 023619 (2008).
[16] M. Horikoshi and K. Nakagawa, Phys. Rev. Lett. **99**, 180401 (2007).
[17] O. Garcia, B. Deissler, K. J. Hughes, J. M. Reeves, and C. A. Sackett, Phys. Rev. A **74**, 031601(R) (2006).
[18] Y. Torii, Y. Suzuki, M. Kozuma, T. Sugiura, T. Kuga, L. Deng, and E. W. Hagley, Phys. Rev. A **61**, 041602(R) (2000).
[19] M. Horikoshi and K. Nakagawa, Phys. Rev. A **74**, 031602(R) (2006).
[20] A. D. Cronin, J. Schmiedmayer, and D. E. Pritchard, Rev. Mod. Phys. **81**, 1051 (2009).
[21] S. Wu, Y.-J. Wang, Q. Diot, and M. Prentiss, Phys. Rev. A **71**, 043602 (2005).
[22] J. A. Stickney, D. Z. Anderson, and A. A. Zozulya, Phys. Rev. A **75**, 063603 (2007).
[23] S. R. Segal, Q. Diot, E. A. Cornell, A. A. Zozulya, and D. Z. Anderson, Phys. Rev. A **81**, 053601 (2010).
[24] J. H. T. Burke and C. A. Sackett, Phys. Rev. A **80**, 061603(R) (2009).
[25] F. Dalfovo, S. Giorgini, L. P. Pitaevskii, and S. Stringari, Rev. Mod. Phys. **71**, 463 (1999).
[26] M. Olshanii and V. Dunjko, e-print arXiv:cond-mat/0505358v2.
[27] J. A. Stickney, R. P. Kafle, D. Z. Anderson, and A. A. Zozulya, Phys. Rev. A **77**, 043604 (2008).
[28] E. O. Ilo-Okeke and A. A. Zozulya, Phys. Rev. A **82**, 053603 (2010).

Index